Mon. Not. R. Astron. Soc. **326,** 959–980 (2001)

Empirical calibration of the near-infrared Ca II triplet – I. The stellar library and index definition

A. J. Cenarro,[1]★ N. Cardiel,[1] J. Gorgas,[1] R. F. Peletier,[2] A. Vazdekis[3] and F. Prada[4]

[1]*Departmento de Astrofísica, Fac. de Ciencias Físicas, Universidad Complutense de Madrid, 28040 Madrid, Spain*
[2]*School of Physics and Astronomy, University of Nottingham, University Park, Nottingham NG7 2RD*
[3]*Department of Physics, University of Durham, South Road, Durham DH1 3LE*
[4]*Observatorio de Calar Alto, Almería, Spain*

Accepted 2001 April 20. Received 2001 February 22; in original form 2000 October 27

ABSTRACT

A new stellar library at the near-IR spectral region developed for the empirical calibration of the Ca II triplet and stellar population synthesis modelling is presented. The library covers the range λλ8348–9020 at 1.5-Å (FWHM) spectral resolution, and consists of 706 stars spanning a wide range in atmospheric parameters. We have defined a new set of near-IR indices, CaT*, CaT and PaT, which mostly overcome the limitations of previous definitions, the former being specially suited for the measurement of the Ca II triplet strength corrected for the contamination from Paschen lines. We also present a comparative study of the new and the previous Ca indices, as well as the corresponding transformations between the different systems. A thorough analysis of the sources of index errors and the procedure to calculate them is given. Finally, index and error measurements for the whole stellar library are provided together with the final spectra.

Key words: stars: abundances – stars: fundamental parameters – globular clusters: general – galaxies: stellar content.

1 INTRODUCTION

With this paper we start a series dedicated to the empirical calibration of the near-IR Ca II triplet. The ultimate aim of this work is to use the strength of the Ca lines in this spectral range to investigate the stellar content of early-type galaxies. However, we expect that researchers in different areas (e.g. starburst and active galaxies, globular clusters, and stellar astrophysics) can make use of some of the results and information that will be presented throughout these papers. These include a new stellar library, a set of homogeneous atmospheric parameters, empirical fitting functions describing the behaviour of the Ca triplet with the stellar parameters, and stellar population model predictions.

Traditionally, elliptical galaxies have been thought to be a uniform class of objects, with global properties changing smoothly with mass and hosting old and coeval stellar population. However, over the last decade, a growing body of evidence is indicating that the formation processes and star formation histories of, at least, an important fraction of early-type galaxies are much more complex and heterogeneous. The apparent age spread among elliptical galaxies (González 1993; Faber et al. 1995; Jørgensen 1999), the distribution of element abundances (Worthey 1998; Peletier 1999; Trager et al. 2000a) and the interpretation of the scaling relations (like the colour–magnitude or $Mg_2-\sigma$ relations; Bower, Lucey & Ellis 1992; Bender, Burstein & Faber 1993; Pedraz et al. 1999; Terlevich et al. 1999; Kuntschner 2000; Trager et al. 2000b), are some of the main issues in the present debate about the evolutionary status of early-type galaxies. A major common obstacle to tackle with the previous problems is how to disentangle age and metallicity effects in the integrated spectrum of a composite stellar population.

The measurement and interpretation of line-strength indices in the spectra of early-type galaxies has been a fundamental tool to address the above topics, the Lick/IDS (Image Dissector System) system (Worthey et al. 1994 and references therein) being the most widely used (but see also Rose 1994). The Lick system makes use of strong spectral features in the blue spectral range (from λ4100 to λ6300), although only the main absorption lines in the narrower λλ4800–5400 range have been extensively measured with high precision in the spectra of early-type galaxies. More recently, new spectral indices have been defined and calibrated in the bluer region (Jones & Worthey 1995; Worthey & Ottaviani 1997; Gorgas et al. 1999; Vazdekis & Arimoto 1999), with enlarged capability to decouple age and metallicity effects. However, the spectral range of interest is still quite narrow. It is obvious that enlarging the wavelength coverage will allow us to investigate the relative contributions of different stellar types to the composite spectrum. As an example, a comparison between the mean ages derived

★E-mail: cen@astrax.fis.ucm.es

using, as an age discriminant, features in different spectral regions, can provide important constraints about the star formation history of the galaxies (Sánchez-Blázquez et al. 2000). Although an important effort has been made to extend the stellar population studies to the ultraviolet region (e.g. Ponder et al. 1998), this is not the case for the near-IR. In fact, it is remarkable that, although the features in the near-IR spectral range were already included in the early analyses of the extragalactic old stellar populations (e.g. Spinrad & Taylor 1971), 30 yr later, and despite the advent of modern charge-coupled device (CCD) detectors, the potential of this spectral range to investigate the stellar population of early-type galaxies is still almost unexploited.

The Ca II triplet is one of the most prominent features in the near-IR spectrum of cool stars and its potential to study the properties of stellar populations has been extensively acknowledged in the literature (see Section 2.2 for a review of previous works on the subject). However, a reliable analysis of the Ca triplet measurements in integrated spectra rests on the comparison of the data with the predictions of stellar population models. The accuracy of such predictions is highly dependent on the input calibration of the Ca line-strengths in terms of the main atmospheric stellar parameters (namely effective temperature, surface gravity and metallicity). The quality of this calibration has been the major drawback of previous stellar population models which have included predictions for the strength of the Ca triplet (Vazdekis et al. 1996; Idiart, Thévenin & de Freitas Pacheco 1997, hereafter ITD; Mayya 1997; García-Vargas, Mollá & Bressan 1998; Mollá & García-Vargas 2000; Schiavon, Barbuy & Bruzual 2000). Previous calibrations have been either theoretical (based on model atmospheres), with their associated uncertainties, or based on empirical stellar libraries with a poor coverage of the atmospheric parameter space. Apart from this major problem, there are other factors which have compromised, with different impacts, the reliability of these previous papers. They include stellar libraries with too few stars, problematic index definitions (e.g. they cannot be used for all spectral types), uncertainties in the input stellar parameters (which translate into unknown uncertainties in the derived predictions), and illnesses in the fitting procedures (a proper statistical analysis of the computed coefficients is seldom followed). Throughout this work we will review and comment in detail on all these problems and how we have coped with them.

The main motivation of the present series of papers is, therefore, to provide a reliable calibration of the near-IR Ca II triplet that makes it possible to accurately calculate the behaviour of the Ca line-strengths in stellar populations with a wide range of ages and metallicities. The outline of the series is as follows. In this first paper we introduce the new stellar library and define a new set of indices to quantify the strength of the Ca triplet. Cenarro et al. (2001a; hereafter Paper II) is dedicated to the determination of the input atmospheric parameters for the stellar sample. These are some of the basic ingredients of the empirical fitting functions and the spectral synthesis analysis that will be presented in Cenarro et al. (2001b; hereafter Paper III) and Vazdekis et al. (in preparation; hereafter IV), respectively. In this latter paper, we will compute the predictions for single-burst stellar population models in two parallel ways: providing the Ca triplet strength using the fitting functions of Paper III, and supplying spectral energy distributions in the λλ8348–9020 range (following Vazdekis 1999).

In Section 2 of this paper we review previous work on the Ca II triplet behaviour and its applications to different astrophysical problems. Section 3 describes the new stellar library as well as an overview of the observation and reduction procedures. A thorough discussion of the Ca II index definition is given in Section 4, where we define new improved Ca II indices which overcome the problems affecting previous definitions. This section also includes a comparative study of the sensitivity of the Ca II indices to effects like the signal-to-noise (S/N) ratio or the spectral resolution, and a set of calibrations for converting between different index definitions. In Section 5, an extensive analysis of index errors is presented, discussing the different sources of random errors and systematic effects. As a supplement of this section, Appendix A provides accurate formulae for the computation of random errors in the index measurements, together with an analytical estimate of errors from S/N ratios. Finally, in Section 6 we refer the reader to a web page in which we provide a data base containing the spectra for the whole library, an electronic table listing full information for each star, and public FORTRAN routines to compute the new indices and their associated errors.

2 PREVIOUS WORKS ON THE NEAR-IR CA II TRIPLET

In a pioneer work, Merrill (1934) (see also Wilson & Merrill 1937) explored for the first time the near-IR region of stellar spectra, identifying the most relevant absorption features and noting that *the lines of* Ca IIλλ8498, 8542, 8662 are prominent in types A–M and may have an interesting relationship to absolute magnitude. This tentative prediction was confirmed by the subsequent works of Keenan & Hynek (1945) and Parsons (1964). In particular, the latter showed how the strength of the Ca lines (blended with Paschen lines for early-type stars) increases with absolute magnitude (i.e. being larger for supergiants) at fixed spectral type. Later works by O'Connell (1973), Anderson (1974), Cohen (1978), and others (see below) confirmed these findings, establishing the near-IR Ca triplet as one of the most striking luminosity-sensitive features in the spectra of F–M stars.

2.1 Calibrations of the Ca line-strengths

After these early studies, several authors have tried to model the behaviour of the Ca triplet with the basic atmospheric parameters ($T_{\rm eff}$, $\log g$ and [Fe/H]). Two main lines of approach have been followed, either using empirical stellar libraries, or using the predictions of stellar atmosphere models.

2.1.1 Empirical calibrations

Among the works following the empirical method, we must remark on that of Jones, Alloin & Jones (1984, hereafter JAJ), in which they found that the Ca triplet strength strongly correlates with gravity (in the sense that it increases for giant and supergiant stars). They also noted that the residuals of this relation correlate weakly with metallicity. This strong gravity dependence was independently confirmed by Carter, Visvanathan & Pickles (1986) and Alloin & Bica (1989), although they did not agree in their conclusions about the metallicity dependence, being stronger in the latter study.

An important step to quantify the g and [Fe/H] dependence was given by the comprehensive study of Díaz, Terlevich & Terlevich (1989, hereafter DTT). Using a stellar library with an enlarged range in gravity and metallicity, these authors quantified the biparametric behaviour with $\log g$ and [Fe/H], noting that, in the high-metallicity range, the strength of the Ca triplet depends only

on gravity, whilst, for low-metallicity stars, [Fe/H] is the main parameter. Zhou (1991, hereafter ZHO) carried out a similar analysis, using a higher spectral resolution (2 Å) and extending the sample of stars by including cooler stars (up to M7). He found that the effect of temperature, found to be negligible in the previous work, was important at low $T_{\rm eff}$. He also noted that the gravity dependence was stronger for giants than for dwarfs.

Another relevant study is that of Mallik (1994, 1997). Through the analysis of an ample stellar library at high resolution (0.4 Å), this author confirmed the strong dependence on $\log g$ (and showed that it was stronger as metallicity increases) and the milder dependence on [Fe/H] (but, remarkably, more important for supergiant stars, in agreement with DTT). Unfortunately, he does not provide any fitting function, restricting the potential application of these qualitative results. ITD have derived empirical functions which predict the strength of the Ca triplet in terms of the three atmospheric parameters. Using a library with a good coverage in metallicity but lacking a representative sample of supergiants, they conclude that gravity dependence is not as strong as previously reported, and that metallicity is the main parameter.

It is clear that there are some apparent contradictions among the conclusions of these papers. A critical analysis of these will be presented in Paper III of this series, where we will show that the apparent discrepancies are mainly because of the different ranges of stellar parameters in the employed stellar libraries, the diversity of index definitions (see Section 4.2), and differences in the fitting procedures (e.g. in most cases, a proper statistical approach was not applied).

2.1.2 *Theoretical calibrations*

The theoretical modelling of the Ca triplet lines is not simple since the line cores are formed in the stellar chromosphere and, therefore, non-local thermodynamic equilibrium (NLTE) models are required. For this reason, the first attempts to analyse the sensitivity of the Ca strength to the atmospheric parameters were restricted to the line wings. In this sense, Smith & Drake (1987, 1990) concluded that the dependence on metallicity should be larger than that reported by the empirical studies (like JAJ), and that effective temperatures had a non-negligible effect. Erdelyi-Mendes & Barbuy (1991), also using LTE models, extended the analysis to cooler stars and included the significant contribution of molecular bands. They agreed with Smith & Drake in that metallicity, rather than gravity, was the main parameter, the [Fe/H] dependence being stronger for lower gravities.

Using NLTE models, Jørgensen, Carlsson & Johnson (1992) carried out, for the first time, the computation of the line cores, deriving full equivalent-widths. (They showed, however, that the effects of departures from LTE are negligible since the equivalent widths are dominated by the line wings.) Concerning the sensitivity to stellar parameters, they found that the gravity dependence of the Ca triplet is influenced by $T_{\rm eff}$ and [Fe/H] in a complicated way. They provided fitting functions for stars in the range $4000 \leq T_{\rm eff} \leq 6600$ K and $-1.0 \leq$ [A/H] $\leq +0.2$ dex.

Recently, Chmielewski (2000) has presented a comprehensive analysis of the theoretical modelling of the Ca lines. He stresses that previous works did not take into account the contribution of hydrogen Paschen lines to the integrated equivalent widths, showing that this contribution is significant for dwarfs hotter than 5800 K and giants with $T_{\rm eff}$ above ~5500 K. Interestingly, this effect explains most of the discrepancies between the previous empirical and theoretical works concerning the temperature dependence of the Ca lines. His main conclusions about the Ca line-strength sensitivity to the stellar parameters are that the gravity dependence only holds for $\log g < 3$ dex, metallicity is a significant parameter in all cases, and temperature effects can only be neglected for dwarfs between 5000 and 6000 K.

Unfortunately, these theoretical studies, being very important to help to understand the behaviour of the Ca triplet and to check the empirical studies, are restricted to cool stars (typically between F and K) and, obviously, their conclusions cannot be extrapolated to later spectral types to construct stellar population synthesis models of, relatively old, stellar systems.

2.2 Applications of the Ca triplet to the study of stellar systems

Over the years, the near-IR Ca triplet has been used extensively to address a number of topics in different areas.

2.2.1 *Stellar astrophysics*

In the field of stellar astrophysics, the triplet, together with other spectral features in this spectral range, has been used for the spectral classification of stars (Sharpless 1956; Bouw 1981; Kirkpatrick, Henry & McCarthy 1991; Ginestet et al. 1994; Munari & Tomasella 1999). These features have also been widely used as chromospheric activity indicators (e.g. Linsky et al. 1979; Dempsey et al. 1993; Montes et al. 1998). Furthermore, its sensitivity to surface gravity has been exploited to identify supergiants in the Galaxy (e.g. Garzón et al. 1997) or in the Local Group galaxies (Mantegazza 1992; Humphreys et al. 1988; Massey 1998).

2.2.2 *Globular clusters*

In spite of the first empirical papers which remarked that the Ca triplet was mainly gravity driven (see above), Armandroff & Zinn (1988, hereafter A&Z), in a pioneering study, found that, in the integrated light of galactic globular clusters, the Ca equivalent width was well correlated with metallicity, indicating that this feature could be a fair metallicity indicator for old, and approximately coeval, stellar populations, provided that the metallicity was lower than solar.

Subsequent work in this field concentrated in the study of individual red giants of globular clusters. Armandroff & Da Costa (1991, hereafter A&D) derived an empirical relation between the cluster metallicity and the 'reduced' equivalent width $W' = \mathrm{EW(CaT)} + \mathrm{c}(V - V_{\rm HB})$, where c is a constant term, EW(CaT) is the pseudo-equivalent width (typically the sum of the two strongest lines of the triplet), and $V_{\rm HB}$ is the V magnitude of the horizontal branch. Note that W' is a monotonic function of metallicity because gravity effects are removed by the last term of the equation. This relation has been recalibrated by several authors (e.g. Da Costa & Armandroff 1995; Geisler et al. 1995; Rutledge et al. 1997a, Rutledge, Hesser & Stetson 1997b, hereafter RHS) and extensively used to derive metallicities of galactic globular clusters (Armandroff, Da Costa & Zinn 1992; Da Costa, Armandroff & Norris 1992; Buonanno et al. 1995; Suntzeff & Kraft 1996; Rosenberg et al. 1998), clusters and individual stars in the Magellanic Clouds (Olszewski et al. 1991; Suntzeff et al. 1992; Da Costa & Hatzidimitriou 1998; Cole, Smecker-Hane & Gallagher 2000), and Local Group dwarf spheroidals (Suntzeff et al. 1993; Smecker-Hane et al. 1999). A comprehensive analysis

of the different methods to measure cluster metallicities using the Ca triplet can be found in RHS.

2.2.3 *Active galaxies and extragalactic H II regions*

One of the fields in which the study of the Ca triplet has had a wide application is that of active galaxies and starburst regions. Terlevich, Díaz & Terlevich (1990a) studied the Ca triplet in a sample of normal and active galaxies, concluding that low-ionization nuclear emission regions (LINERS) and Seyfert 2 objects exhibit Ca strengths equal or larger than those found in normal ellipticals (in contrast with the blue absorption lines, which are usually diluted in active galaxies). Following the conclusion of DTT that Ca equivalent widths above 9 Å are only found in red supergiant stars, they interpret this result as a strong evidence for the occurrence of nuclear starbursts in the central regions of active galaxies. This same approach has been followed by a number of authors (Forbes, Boisson & Ward 1992; García-Vargas et al. 1993; González Delgado & Pérez 1996a,b; Heckman et al. 1997; Pérez et al. 2000) to study the evolutionary status of the nuclei and circumnuclear regions of active galaxies through the presence of red supergiants.

The Ca triplet has also been detected in extragalactic H II regions (Terlevich et al. 1990b, 1996), being interpreted as a result of the recent star formation burst, and it has been used to study the star formation history of extragalactic superstar clusters (Prada, Greve & McKeith 1994; García-Vargas et al. 1997; González Delgado et al. 1997; Gallagher & Smith 1999; Goudfrooij et al. 2001).

2.2.4 *Early-type galaxies*

The first papers analysing the Ca triplet in early-type galaxies tried to make use of its gravity sensitivity to constrain the dwarf/giant ratio in the integrated light of old stellar populations. The main debate at that time was focused on the possible dwarf enrichment in the nucleus of M 31, as compared to its bulge or to low-luminosity ellipticals like M 32. While Faber & French (1980) and, to some degree, Carter et al. (1986) favoured a dwarf-enriched stellar population, Cohen (1978) and Alloin & Bica (1989) found that metallicity effects and contamination by a molecular band could account for the apparent enrichment, mainly based on measurements of the strength of the Na I feature at λ8190.

One interesting result from these first studies was that it was found that the strength of the Ca triplet did not vary much among early-type galaxies (Cohen 1979). Note that although Cohen (1978) found that the nucleus of M 31 exhibited stronger Ca lines than M 32, Faber & French (1980) reported the opposite behaviour. Later, Bica & Alloin (1987, hereafter B&A) measured the Ca strength in the spectra of 62 galactic nuclei (from E to Sc), concluding that the equivalent widths were not related to galaxy types or luminosities. This was confirmed by the studies of Terlevich et al (1990a), in which they found a small spread in the Ca strengths of 14 normal galaxy nuclei, and Houdashelt (1995), who noted that the Ca equivalent widths of a sample of 34 early-type galaxies did not vary significantly among galaxies of different colour or absolute magnitude.

The apparent uniformity of the Ca measurement in elliptical galaxies is somewhat surprising since: (i) it contrasts with the metallicity dependence found for the stellar samples and the reported behaviour in galactic globular clusters (see above), (ii) previous stellar population models predict a high sensitivity of the Ca triplet to the metallicity of metal rich old stellar populations (García-Vargas et al. 1998; Schiavon et al. 2000), and (iii) it has been argued that, in contrast to other α-elements, Ca abundance is not enhanced compared to Fe in bright elliptical galaxies (O'Connell 1976; Vazdekis et al. 1997; Worthey 1998; Mollá & García-Vargas 2000), and variations of the Fe line-strengths among ellipticals, although difficult to detect, are not negligible (e.g. Gorgas, Efstathiou & Aragón–Salamanca 1990; Davies, Sadler & Peletier 1993; González 1993; Kuntschner 2000). Therefore, more reliable predictions of the Ca triplet behaviour in the integrated stellar population of high-metallicity systems and new high-quality measurements are hardly needed to clarify this point.

This problem is closely related to the radial behaviour of the Ca strengths within galaxies. Given the measured metallicity gradients usually found in elliptical galaxies (see González & Gorgas 1996, and references therein), even using Fe line-strengths, one should expect to find unambiguous negative gradients in Ca. However, Cohen (1979) and Boroson & Thompson (1991) found negligible gradients; Carter et al (1986) and Peletier et al. (1999) measured either null or positive gradients, and Delisle & Hardy (1992, hereafter D&H) found negative gradients in many galaxies of their sample.

Another important difficulty arises when we try to compare the absolute values of the Ca triplet measured in early-type galaxies with the actual values predicted by stellar population synthesis models (e.g. Peletier et al. 1999; Mollá & García-Vargas 2000). The uncertainties of the theoretical or empirical Ca behaviour implemented in such models, together with other problems such as observational uncertainties, corrections from velocity dispersion or transformations between different index definitions, make it very difficult to extract any significant conclusion from such a comparison.

3 THE NEAR-IR STELLAR LIBRARY

3.1 Previous libraries in the near-IR spectral range

Previous stellar libraries providing spectra in the Ca II triplet spectral range are listed in Table 1. Here we only include libraries with a spectral resolution better than 10 Å [full width at half-maximum (FWHM)]. For a list of lower resolution libraries we refer the reader to Munari & Tomasella (1999). We have also excluded from this list some libraries which are too specific for the purposes of this work, like those of Fluks et al. (1994) (only M stars), Allen & Strom (1995) (stars from two open clusters), RHS (huge collection of red giants from galactic globular clusters), or Montes & Martín (1998) (high-resolution library in a limited spectral range). It is clear from this table that no previous library provides simultaneously a broad coverage of stellar metallicities and effective temperatures. In fact, the only libraries including a good fraction of low-metallicity stars are those of DTT and ITD, but the spectral type ranges spanned in these cases are rather limited, especially in the latter case (as we will see in Paper IV, the relative contribution of stars colder than K3 to the near-IR spectrum of an old stellar population is very important). On the other hand, libraries composed of stars of all spectral types do not attain a broad range in metallicity (e.g. Munari & Tomasella 1999). The low frequency of supergiant stars is an additional problem of some libraries (JAJ; ITD). It must be noted that some of the apparent discrepancies among different authors who have modelled the behaviour of the CaT index with the atmospheric parameters are mainly because of this different coverage of the parameter space by the calibrating stars (see Paper III).

3.2 The sample

We have observed a new stellar library of 706 stars at the near-IR spectral region (λλ8348–9020). It includes 421 of the 424 stars with known atmospheric parameters of the Lick/IDS Library (Burstein et al. 1984; Faber et al. 1985; Burstein, Faber & González 1986; Gorgas et al. 1993; Worthey et al. 1994). This subsample spans a wide range in spectral types and luminosity classes. Most of them are field stars from the solar neighbourhood, but stars covering a wide range in age (from open clusters) and with different metallicities (from galactic globular clusters) are also included. In order to obtain a large sample of stars in common with other previous works devoted to the Ca II triplet, our stellar library was enlarged to include 105 of the 106 stars of DTT and 43 of the 55 stars of the sample of ITD. Moreover, with the aim of filling gaps in the parameter space, we also included stars from several other compilations, mainly focusing on O, B and A types (37 hot stars from the sample of Andrillat, Jaschek & Jaschek 1995), late M types, metal poor, metal rich and chemically peculiar stars (40 stars from a list kindly provided by G. Worthey, private communication, and 102 stars from Jones 1997). The presence of hot stars in the stellar library allows us to expand the predictions of our models to young stellar populations. Also, and as it will be shown in Paper IV, very cool stars are necessary to reproduce the integrated spectra of old stellar systems at the near-IR spectral region over a wide range of ages. Finally, since Ca is an α-element, 29 additional stars with high or low Ca/Fe ratios from the catalogue of Thévenin (1998) were observed in order to analyse the Ca II index dependence on relative abundances (see Paper III).

The new stellar library covers the following ranges in atmospheric parameters: $T_{\rm eff}$ from 2750 to 38400 K, $\log g$ from 0 to 5.12 dex, and [Fe/H] from −3.45 to +0.60 dex. It is important to note that the stars of the stellar library do not homogeneously cover the parameter space. In fact, most of the stars (∼83 per cent) have metallicities from −1.0 to +0.5 dex, and the widest gravity range is also within this metallicity interval. The final atmospheric parameters which have been adopted for each star and the method to derive them are discussed in detail in Paper II of this series. We refer the reader to that paper for an HR diagram of the whole sample.

3.3 Observations and data reduction

The spectra of the stellar library were obtained during a total of 21 nights in six observing runs from 1996 to 1997 using the Jacobus Kapetyn Telescope (JKT), Isaac Newton Telescope (INT) and William Herschel Telescope (WHT) at the Roque de los Muchachos Observatory (La Palma, Spain) and the 3.5-m telescope at Calar Alto Observatory (Almería, Spain). It is important to note that most of the stars (∼93 per cent), including all the field stars and the brightest ones from open and globular clusters, were observed during the three runs at the JKT using the same instrumental configuration. This ensures a high homogeneity among the data of these three runs (see the analysis in Section 5.3). The instrumental configuration at the other telescopes was also chosen to be as similar as possible to that at the JKT, obtaining spectral resolutions (FWHM) for the six runs in the range from 1.07 to 2.13 Å. A full description of these and other instrumental details is given in Table 2. We must note that, as it will be explained in Section 5.2, spectra from runs 1, 3 and 4 were broadened to the spectral resolution of run 2 (1.5 Å). Hence, and with the exception of the few stars observed in runs 5 and 6, the whole library has a common resolution. $N_{\rm obs}$ stands for the number of stars observed in each run.

Typical exposure times varied from a few seconds for bright stars to 1800 s for the faintest cluster stars. These ensured typical values of SN(Å) ∼ 100Å^{-1} (S/N ratio per angstrom) for field and open cluster stars, and SN(Å) ≥ 15 for the globular cluster stars. In

Table 1. Medium-resolution stellar libraries in the Ca II triplet spectral region.

Reference	Number of stars	Resolution (FWHM, Å)	Spectral types	[Fe/H] range	Comments
JAJ	62	3	B–M5	−0.60, +0.23	
DTT	106	3.5	F5–M1	−2.70, +0.55	
Zhou (1991)	144	2	F5–M7	−2.28, +0.60	two stars with [Fe/H] < −0.61
Andrillat et al. (1995)	76	1.2	O5–G0		
Serote Roos, Boisson & Joly (1996)	21	1.25	B3–M5	−0.15, +0.39	Only giants and supergiants
Carquillat et al. (1997)	36	2	F5–M4		
Idiart et al. (1997)	55	∼2	A1–K3	−3.15, +0.35	
Mallik (1997)	146	0.4	F7–M4	−3.0, +1.01	one star with [Fe/H] < −1.6
Munari & Tomasella (1999)	131	0.43	O4–M8	−0.54, +0.30	
Montes, Ramsey & Welty (1999)	130	∼0.7	F0–M8	−2.74, +0.31	three stars with [Fe/H] < −0.5
This work	706	1.5	O6–M8	−3.45, +0.60	

Table 2. Observational configurations.

Run	Dates	Telescope	Spectrograph	Detector	Dispersion (Å pixel^{-1})	Δλ (Å)	Slit width (arcsec)	FWHM (Å)	$N_{\rm obs}$
1	1996 September 20–26	JKT 1.0 m	RBS	TEK#4	0.85	8331–9200	1.5	1.18	264
2	1997 January15–19	JKT 1.0 m	RBS	TEK#4	0.85	8331–9200	1.5	1.50	248
3	1997 June 25–29	JKT 1.0 m	RBS	TEK#4	0.85	8331–9200	1.5	1.07	362
4	1997 August 13	INT 2.5 m	IDS	TEK#3	0.85	8185–9055	1.5	1.28	33
5	1996 August 4	WHT 4.2 m	ISIS	TEK#2	0.79	8222–9031	1.2	2.13	12
6	1996 November 17–18	CAHA 3.5 m	TWIN	SITe#4d	0.81	8300–9912	2.1	2.11	15

order to test the derived random errors of the final index measurements (see Section 5.1), we performed multiple observations of a subsample of stars (15–20) within each particular run and in common with other different runs. Finally, to perform a reliable flux calibration, several (3 or 4) spectrophotometric standards were observed along each night at different zenithal distances.

The reduction of the data was performed with $R_E D_m^{uc} E$[1] (Cardiel 1999), which allows a parallel treatment of the data and error frames (see more details in Section 5) and, therefore, produces an associated error spectrum for each individual data spectrum. We carried out a standard reduction procedure for spectroscopic data: bias and dark subtraction, cosmic ray cleaning, flat-fielding, C-distortion correction, wavelength calibration, S-distortion correction, sky subtraction, atmospheric extinction correction, spectrum extraction, and relative flux calibration. We did not attempt to obtain absolute fluxes since both the evolutionary synthesis codes and the line-strength indices only require relative fluxes. Cluster stars were also corrected from interstellar reddening using the colour excesses from Gorgas et al. (1993) and Worthey et al. (1994) and the averaged extinction curve of Savage & Mathis (1979).

In order to optimize the observing time during the JKT runs, we decided not to acquire flat-field and comparison arc frames for each individual exposure of a library star. Concerning the flat-field correction, after checking that small variations of the CCD temperature do not affect the flat-field structure and considering that it exclusively depends on the position of the telescope, we obtained a complete set of flat-field exposures by pointing at a grid of positions on the dome (with a resolution of 30° in azimuth and 15° in altitude) during the day. Later, using the alt-azimuth coordinates of each star, the closest flat-field frame over the whole set was finally used as its own flat-field calibration frame. It is important to highlight the importance of an accurate flat-field correction when the fringe pattern becomes relevant, as it is usually the case in this spectral range. Depending on the properties of the CCD, the fringe effect introduced high-frequency structures with an amplitude of up to 7 per cent of the true flux, but they virtually disappeared on using our procedure. Flux differences between the normalized fringe patterns of different flat-field frames allow an estimation of the uncertainties introduced in the fringe correction procedure. These are always below 0.6 per cent.

Concerning the wavelength calibration, we only obtained comparison arc frames for a previously selected subsample of stars covering all the spectral types and luminosity classes in each run. The selected spectra were wavelength calibrated with their own arc exposures taking into account their radial velocities, whereas the calibration of any other star was performed by a comparison with the most similar, already calibrated, reference spectrum. This working procedure is based on the expected constancy of the functional form of the wavelength calibration polynomial within a considered observing run (which has been widely tested by comparing the derived polynomials for each run). In this sense, the algorithm that we used is as follows: after applying a test x-shift (in pixels) to any previous wavelength calibration polynomial, we obtained a new polynomial which was used to calibrate the spectrum. Next, the calibrated spectrum was corrected from its own radial velocity and, finally, the spectrum was cross-correlated with a reference spectrum of similar spectral type and luminosity class, in order to derive the wavelength offset between both spectra. By repeating this procedure, it is possible to obtain the dependence of the wavelength offset as a function of the test x-shifts and, as a consequence, we derive the required x-shift corresponding to a null wavelength offset. Uncertainties in the wavelength calibration are estimated in Section 5.

It is also important to account for the presence of telluric absorptions, mainly at the red end of the spectral range (the strongest lines are located at λλ8952, 8972, 8980, 8992). Fortunately, since these strong H_2O lines do not affect the Ca II triplet region and the observations were performed under dry conditions, we did not correct for their contamination and it is possible that our final spectra present unremoved features at the red end. An illustrative example of the effect of telluric lines in the Ca II triplet region is given in Stevenson (1994) and Chmielewski (2000).

4 CA II TRIPLET INDICES DEFINITION

Line-strength indices have been widely defined to obtain objective measurements of any relevant spectral feature. For the Ca triplet, there exist previous index definitions from other authors which were optimized to measure the lines for a narrow range of spectral types (mainly G and K types). These previous indices, however, are not appropriate for all the spectral types. Hot and cold stars show strong spectral features which were not taken into account for those index definitions and, as a consequence, most of the Ca measurements for these spectral types become unrealistic. Moreover, some of the previous definitions have not been optimized for composite stellar systems. Some of them require spectra with high S/N ratio, becoming unpractical for faint objects. Besides, some indices show a strong dependence on spectral resolution, or velocity dispersion broadening. In this sense, one should not forget that, in the study of stellar populations, to measure true equivalent widths is not as important as to obtain robust index measurements, specially in spectra with low S/N ratios or with a wide range of spectral resolutions.

In order to cope with the above problems, we have decided to introduce some new Ca II triplet index definitions. Section 4.1 presents an overview of the strongest spectral features in the range from 8350 to 9020 Å. In Section 4.2 we analyse the behaviour and limitations of previous Ca II triplet index definitions for different spectral types. The new indices are defined in Section 4.3, whereas Section 4.4 is reserved to study the dependence of the new and old index definitions on the S/N ratio, the combined effect of spectral resolution and velocity dispersion broadening, and the flux calibration. Finally, in Section 4.5 we present comparisons and calibrations between different Ca II index systems.

4.1 The λλ8350–9020 spectral region

Prior to any index definition, we have explored how the main absorption features in our wavelength range change along the spectral type sequence (Fig. 1). Apart from several atomic lines of intermediate strength, as those of Fe I (λλ8514.1, 8674.8, 8688.6, 8824.2), Mg I (8806.8 Å) and Ti I (8435.0 Å), the Ca II triplet (λλ8498.02, 8542.09, 8662.14) is the strongest feature over a wide range of spectral types (from F5 to M2 approximately) and for all luminosity classes (see Fig. 1c).

The hydrogen Paschen series (λλ8359.0, 8374.4, 8392.4, 8413.3, 8438.0, 8467.3, 8502.5, 8545.4, 8598.4, 8665.0, 8750.5, 8862.8, 9014.9, from P22 to P10, respectively) is apparent in stars hotter than G3 types. Depending on the luminosity class, the strength of this series reaches a maximum for F or A type stars (Andrillat et al. 1995). In the earliest spectral types, where the Ca II

[1] http://www.ucm.es/info/Astrof/reduceme/reduceme.html

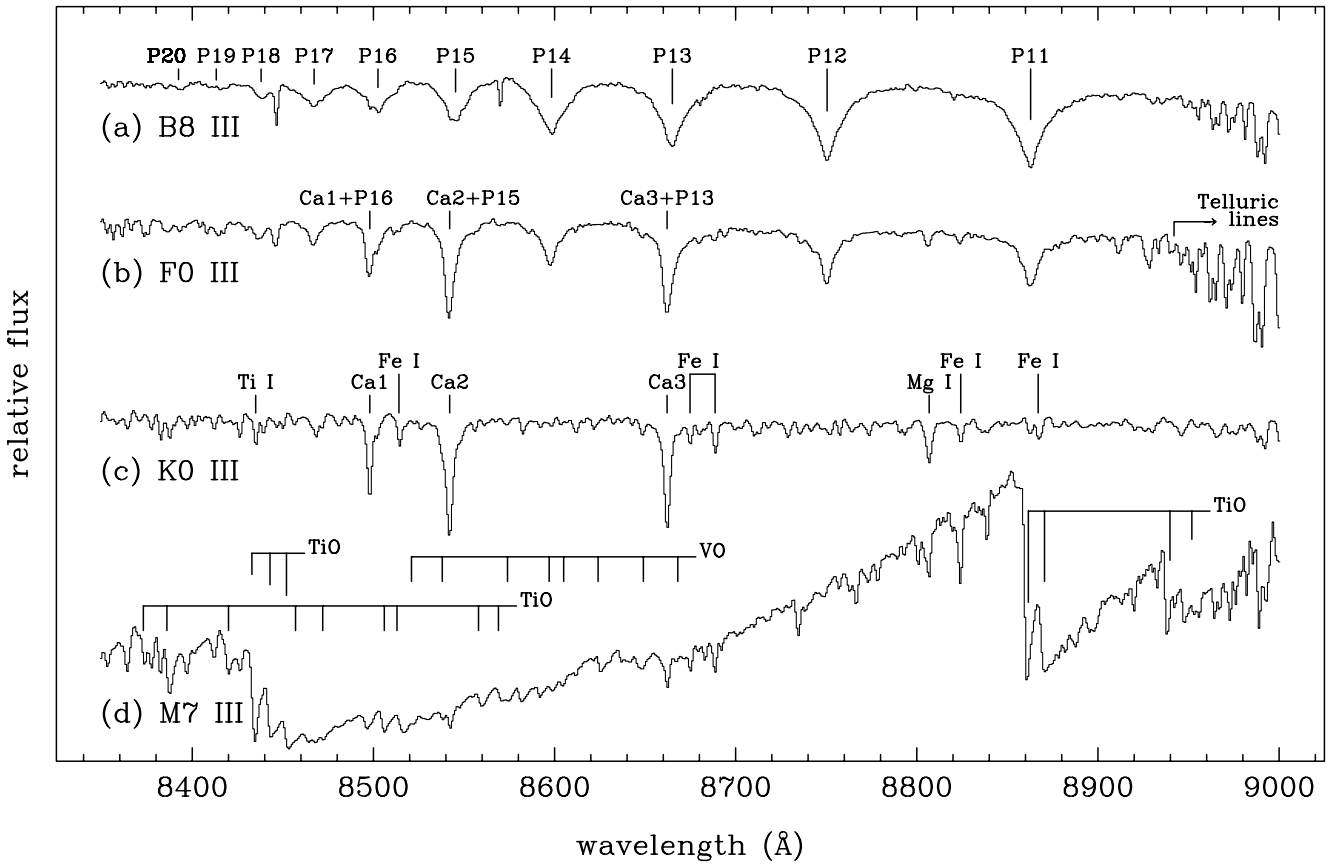

Figure 1. Spectra of the stars HD 186568 (B8 III), HD 89025 (F0 III), HD 216228 (K0 III) and HD 114961 (M7 III) in the spectral range of the stellar library. The strongest features in this region are marked: the Paschen series (from P11 to P20), the Ca II triplet (Ca1, Ca2 and Ca3), several metallic lines (Fe I, Mg I and Ti I), molecular bands (TiO and VO) and telluric absorptions.

strength becomes insignificant, the relative depths of the Paschen lines show a smooth sequence with wavelength (see Fig. 1a). However, because of the fact that, for low and intermediate spectral resolution, the Paschen lines P13, P15 and P16 overlap with the Ca II triplet, these three Paschen lines stand out in the smooth sequence for A and F types (Fig. 1b). The fact that the Ca II lines are blended with the Paschen lines has always been an obstacle to measure the Ca triplet in warm stars (see B&A; Chmielewsky 2000).

Stars cooler than early M types exhibit molecular bands that change the slope of the local continuum (Fig. 1d). The strongest ones are the triple-headed band at λλ8432, 8442, 8452 and the double-headed bands at λλ8859.6, 8868.5 and λλ8937.4, 8949.8 of titanium oxide (TiO). Other molecular features are the band sequence of TiO at λλ8373, 8386, 8420, 8457, 8472, 8506, 8513, 8558, 8569 and several vanadium oxide (VO) bands at λλ8521, 8538, 8574, 8597, 8605, 8624, 8649, 8668 (see Kirkpatrick et al. 1991 and references therein). The strength of these features increases as the temperature decreases, being more prominent for giants than for dwarfs. The spectra of late M type stars are dominated by strong molecular bands showing very weak Ca II lines.

4.2 Previous index definitions

Several previous works have established different index definitions to measure the strength of the Ca II triplet. In particular, the most commonly used indices are those defined by JAJ, B&A, A&Z, DTT, A&D, ZHO, D&H, and RHS. Most of these indices were defined according to the *classical* definition of line-strength indices, that is, by establishing a central bandpass covering the spectral feature of interest, and two other bandpasses (at the red and blue sides of the central region) which are used to trace a local continuum reference level through a linear fit to the mean values in both bands. (For more details about the definition and computation of classical indices see Appendix A1.) In Table 3 we list the limits of bandpasses of the previous definitions.

It must be noted that some of these indices slightly differ from the classical definition. On one hand, the continuum by ZHO is computed from the mean value of the five highest pixels in each continuum bandpass, whereas in the index by JAJ, it is chosen relative to the maximum flux around two selected wavelengths. It is important to stress that this kind of index definitions is useless for low S/N spectra, leading to a spurious negative correlation between index value and S/N ratio. Also, since the classical index definition refers to the measurement of a unique spectral feature, previous definitions are given for each Ca II line. In this sense, the most general Ca II triplet index is usually computed as the sum of the three single-line indices, although some authors (DTT; A&D; ZHO) prefer to use the sum of the two strongest lines of the triplet (λλ8498.0 and 8542.1) or even a weighted combination of the three lines (RHS) in order to optimize the sensitivity of the index to the S/N ratio.

Fig. 2 illustrates both the bandpass position and the predicted continuum of some definitions over three different spectral types. The indices by B&A and RHS have not been included since their blue bandpasses are out of our spectral range. Also the index by A&D has been excluded because of its similarity to the index by A&Z.

Table 3. Limits of bandpasses for previous Ca indices. Codes are the following: JAJ (Jones, Alloin & Jones 1984), B&A (Bica & Alloin 1987), A&Z (Armandroff & Zinn 1988), DTT (Díaz, Terlevich & Terlevich 1989), A&D (Armandroff & Da Costa 1991), ZHO (Zhou 1991), D&H (Delisle & Hardy 1992), and RHS (Rutledge et al. 1997a). Due to the subjective continuum definition by JAJ, bandpasses limits for this index are as given in D&H.

Index	Central bandpass (Å)	Continuum bandpasses (Å)
Ca1(JAJ)	8483.0–8511.0	8633.0–8637.0, 8903.0–8907.0
Ca2(JAJ)	8517.0–8559.0	8633.0–8637.0, 8903.0–8907.0
Ca3(JAJ)	8634.0–8683.0	8633.0–8637.0, 8903.0–8907.0
Ca1(B&A)	8476.0–8520.0	8040.0–8160.0, 8786.0–8844.0
Ca2(B&A)	8520.0–8564.0	8040.0–8160.0, 8786.0–8844.0
Ca3(B&A)	8640.0–8700.0	8040.0–8160.0, 8786.0–8844.0
Ca1(A&Z)	8490.0–8506.0	8474.0–8489.0, 8521.0–8531.0
Ca2(A&Z)	8532.0–8552.0	8521.0–8531.0, 8555.0–8595.0
Ca3(A&Z)	8653.0–8671.0	8626.0–8650.0, 8695.0–8725.0
Ca1(DTT)	8483.0–8513.0	8447.5–8462.5, 8842.5–8857.5
Ca2(DTT)	8527.0–8557.0	8447.5–8462.5, 8842.5–8857.5
Ca3(DTT)	8647.0–8677.0	8447.5–8462.5, 8842.5–8857.5
Ca1(ZHO)	8488.0–8508.0	8447.0–8462.0, 8631.0–8644.0
Ca2(ZHO)	8532.0–8552.0	8447.0–8462.0, 8631.0–8644.0
Ca3(ZHO)	8652.0–8672.0	8447.0–8462.0, 8631.0–8644.0
Ca2(A&D)	8532.0–8552.0	8474.0–8489.0, 8559.0–8595.0
Ca3(A&D)	8653.0–8671.0	8626.0–8647.0, 8695.0–8754.0
Ca1(D&H)	8483.0–8511.0	8559.0–8634.0, 8683.0–8758.0
Ca2(D&H)	8517.0–8559.0	8559.0–8634.0, 8683.0–8758.0
Ca3(D&H)	8634.0–8683.0	8559.0–8634.0, 8683.0–8758.0
Ca1(RHS)	8490.0–8506.0	8346.0–8489.0, 8563.0–8642.0
Ca2(RHS)	8532.0–8552.0	8346.0–8489.0, 8563.0–8642.0
Ca3(RHS)	8653.0–8671.0	8563.0–8642.0, 8697.0–8754.0

In order to predict a reliable local continuum, the continuum bandpasses should be located in spectral regions free from strong absorption features. In this sense, all the previous definitions are optimized for the G and K spectral types (see Figs 2b, 2e, 2h, 2k and 2n). However, because the relative contribution of the earliest spectral types to the integrated spectrum of stellar systems was expected to be negligible at this spectral range, most of the previous Ca indices were defined without taking into account the wavelength position of the Paschen series. The indices by A&Z, DTT and D&H clearly suffer from such a limitation deriving a continuum level below the true one for hot stars (see Figs 2d, 2g, and 2m). On the other hand, because of the presence of molecular bands in late-type stars, some definitions show unreliable continuum levels for these spectral types. In particular, the red bandpass of the index by JAJ falls in a strong TiO absorption (Fig. 2c), while the blue bandpasses by DTT and ZHO (which are roughly the same) are located too close to the continuum break, causing a rise in the continuum level at the position of the Ca lines (see Figs 2i and 2l). Also, when the relative distance between the two continuum bandpasses is too large, the index can be insensitive to local variations in the true continuum (JAJ; DTT), whereas indices with continuum sidebands which are too close (A&Z) are highly sensitive to the velocity dispersion broadening (see Section 4.4.2). As far as the width of the sidebands is concerned, bandpasses that are too wide (D&H) are not appropriate when the spectral region is full of absorption lines which decrease the continuum level. Indices with two narrow sidebands (JAJ) are very sensitive to the S/N ratio and to residuals from sky subtraction. Another important factor is the width of the central bands, since, as we will see in Section 4.4, it mainly determines the sensitivity of the index to the S/N ratio and the velocity dispersion broadening. Finally, and not the least important, it is obvious that any Ca index definition following the classical system is unavoidably affected by Paschen contamination in the central bandpass for stars hotter than G1 and G3, for dwarfs and giants, respectively.

4.3 New indices definitions

Although the previous index definitions have been very useful to increase the understanding of the behaviour of the Ca II triplet both in individual stars and stellar populations (see Section 2), in this work we have decided to define a new set of improved indices, specially designed to be measured in the integrated spectra of galaxies. With the new definitions we have tried to alleviate difficulties such as the continuum definition, the Paschen contamination, and the sensitivity to the S/N ratio and the velocity dispersion (spectral resolution). Note that the aim of these new indices is not to provide measurements as close as possible to the true equivalent widths. Other indices, like those of RHS are much more appropriate for that purpose.

The new indices have been defined according to a new type of line-strength index concept: the *generic* index. It is a natural generalization of the classical definition which includes the following requirements: it is characterized by an arbitrary number of continuum and spectral-feature bandpasses, the contribution of each spectral-feature bandpass can be modified by defining a multiplicative factor for each one, and the pseudo-continuum is derived by using an error weighted least-squares fit to all the pixels of the continuum bandpasses. Although at first sight it could seem that this approach is exactly the same as the one obtained by adding several classical indices (weighted with the corresponding multiplicative factors), the fact that all the spectral features share the same continuum has an important effect in the computation of the index error as is explained in Appendix A2. It is also convenient to highlight that the requirements incorporated in the definition of generic indices translate into important improvements.

(i) Generic indices are specially suited for the measurement of adjacent spectral features, where the use of a common continuum level can be useful. They are also highly recommended when the spectral region of interest is densely populated by spectral features, since many thin continuum bandpasses at adequate locations make it possible to avoid the presence of the other spectral features. Moreover, a large number of continuum bands guarantees a low sensitivity to the S/N ratio and a robust continuum definition.

(ii) As we will prove later, the multiplicative factors are useful to remove the contamination by other spectral features (either in absorption or in emission).

(iii) The use of an error weighted least-squares fit in the determination of the local pseudo-continuum is specially advantageous when we measure the near-IR absorption features. In this spectral region, the presence of sky emission lines and telluric absorptions implies that the S/N ratio, as a function of wavelength, is a highly inhomogeneous function.

Following the notation from Cohen (1978) for the Ca triplet, the new generic index will be referred to as CaT. It is defined by establishing five continuum bandpasses, and three central

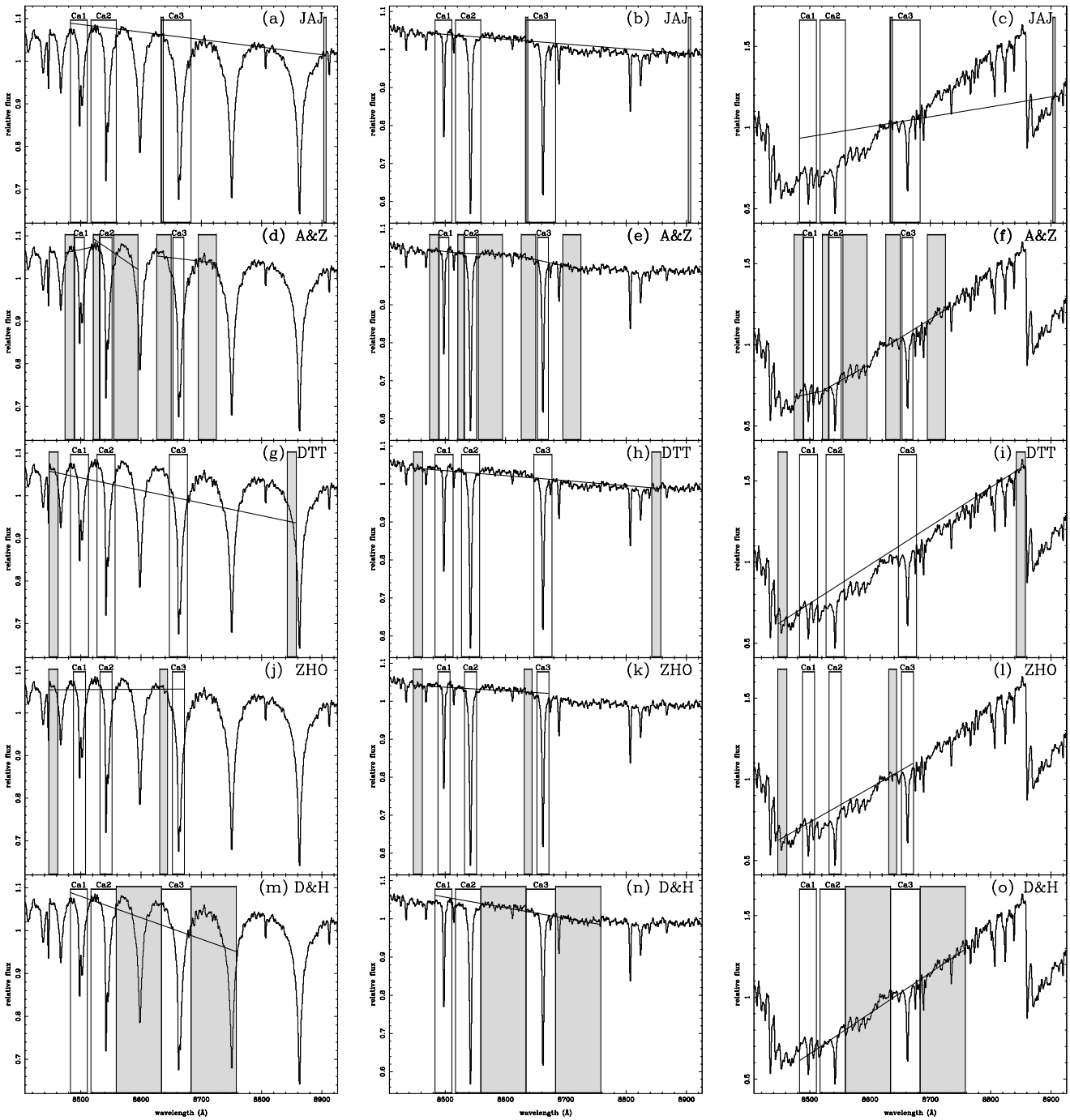

Figure 2. Previous Ca index definitions over different spectral types. Indices (from top to bottom) correspond to the systems of JAJ, A&Z, DTT, ZHO and D&H. The representative spectra (from left to right) are those of HD 161817 (A2 VI), HD 25329 (K1 Vsb) and HD 148783 (M6 III). Grey and open bands mark, respectively, continuum and central bandpasses, whereas the solid line represents the local pseudo-continuum computed by an error weighted least-squares fit to all the pixels in the continuum bands.

bandpasses covering each Ca line (Ca1, Ca2 and Ca3). The continuum regions were carefully chosen to optimize the continuum level for all the spectral types, even when the spectra were broadened up to $\sigma = 300\,\mathrm{km\,s^{-1}}$. In order to calibrate the CaT contamination by the Paschen series in early spectral types, we defined a new generic index, namely PaT, which measures the strength of three Paschen lines free from the Ca contamination. The continuum bandpasses are the same as in CaT whereas the spectral-feature bandpasses (Pa1, Pa2 and Pa3) are centred on the lines P17, P14 and P12 of the series. In both definitions, the multiplicative factors equal unity and the analytical expressions are

$$\mathrm{CaT} = \mathrm{Ca1} + \mathrm{Ca2} + \mathrm{Ca3}, \quad (1)$$

and

$$\mathrm{PaT} = \mathrm{Pa1} + \mathrm{Pa2} + \mathrm{Pa3}. \quad (2)$$

The limits of bandpasses for the CaT and PaT indices are listed in Table 4, and the bandpasses positions and predicted continua are illustrated in Fig. 3 for different spectral types.

Table 4. Limits of bandpasses for the generic indices CaT and PaT.

CaT central bandpasses (Å)	PaT central bandpasses (Å)	Continuum bandpasses (Å)
Ca1 8484.0–8513.0	Pa1 8461.0–8474.0	8474.0–8484.0
Ca2 8522.0–8562.0	Pa2 8577.0–8619.0	8563.0–8577.0
Ca3 8642.0–8682.0	Pa3 8730.0–8772.0	8619.0–8642.0
		8700.0–8725.0
		8776.0–8792.0

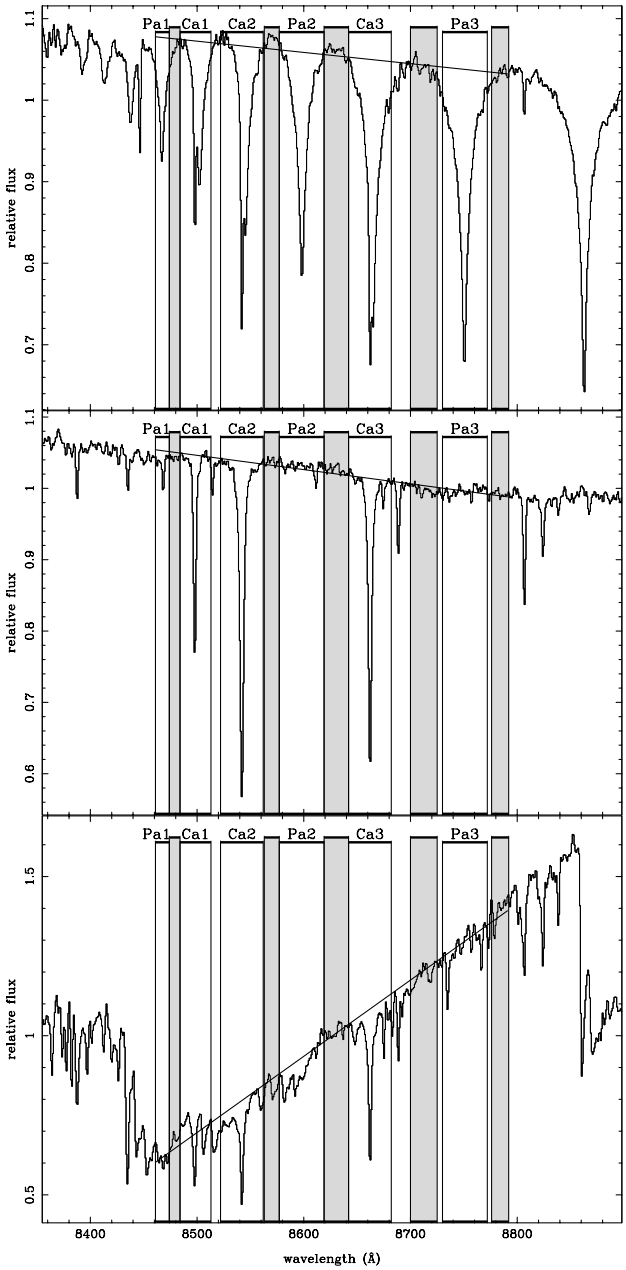

Figure 3. CaT and PaT indices over different spectral types. The spectra correspond (from top to bottom) to HD 161817 (A2 VI), HD 25329 (K1 Vsb) and HD 148783 (M6 III), which are the same spectral types displayed in Fig. 2. Grey and open bands represent continuum and central bandpasses respectively, with the solid line showing the derived local pseudo-continuum.

It is important to note that, apart from rough corrections applied to the integrated spectra of young star clusters (Alloin & Bica 1989) and theoretical considerations on synthetic spectra (Chmielewski 2000), few previous works have faced the Paschen contamination in individual stars.

Finally, we have defined a new Ca triplet index, namely CaT*, which expresses the strength of the Ca II lines corrected from the contamination by Paschen lines. The new index was defined by imposing the following requirements. First, the values of CaT* should be very similar to those of CaT for late-type stars. Secondly, since the true Ca strength in hot stars is very low or even null, the CaT* index should tend to values around zero for the earliest spectral types. Note that, since the CaT index in hot stars is actually measuring the strength of the Paschen lines rather than those of Ca, such an index (as well as those used in previous works) can lead to wrong conclusions when interpreting the integrated spectra of young stellar populations.

To estimate the hydrogen contribution to the Ca index, we have compared the CaT and PaT indices for hot stars, which show a pure smooth Paschen series in their spectra. For this subsample, we should expect a linear relationship between the CaT index (which measures the P16, P15 and P13 lines falling in the Ca1, Ca2 and Ca3 bandpasses) and the PaT index (measuring the P17, P14 and P12 lines). Such a relation was calibrated by using an error weighted least-squares fit to the 26 library stars with $T_{\rm eff} > 10500$ K (see Fig. 4) obtaining

$$\mathrm{CaT} = (0.93 \pm 0.03)\,\mathrm{PaT}. \quad (3)$$

Thus the Paschen corrected CaT* index was defined by subtracting from CaT the correction term given by the above equation, i.e.

$$\mathrm{CaT}^* = \mathrm{CaT} - 0.93\,\mathrm{PaT}, \quad (4)$$

which can be considered, in turn, as a generic index with five continuum bands, six central bandpasses and two different multiplicative factors (1.00 and −0.93). Since we are adopting a definition, the multiplicative factor of −0.93 is assumed to be exact, so we are not concerned with the nominal error of 0.03 obtained in the fit to the hot stars.

Finally, it is worth noting that CaT* is also useful for late-type stars where PaT takes values around zero and the correction term becomes negligible.

For those readers interested in measuring the new indices in their spectra, we provide a set of public FORTRAN subroutines available from the website given at the end of the paper.

4.4 Sensitivities of the indices to different effects

In this section, we discuss the sensitivity of the new and previous Ca indices to the S/N ratio, velocity dispersion broadening (or spectral resolution), relative flux calibration and sky subtraction.

4.4.1 S/N ratio

In Appendix A we show in detail how to compute random errors, arising from photon statistics, for the new generic indices. Following a procedure similar to that presented in Cardiel et al. (1998, hereafter CGCG), we have derived accurate formulae for the computation of random errors for the new Ca indices (Appendix A2). Note that reliable random errors can only be derived when, after a full control of the error propagation throughout the data reduction, an accurate error spectrum is derived for each data spectrum. Appendix A3 also provides analytical estimates of the predicted random errors as a function of

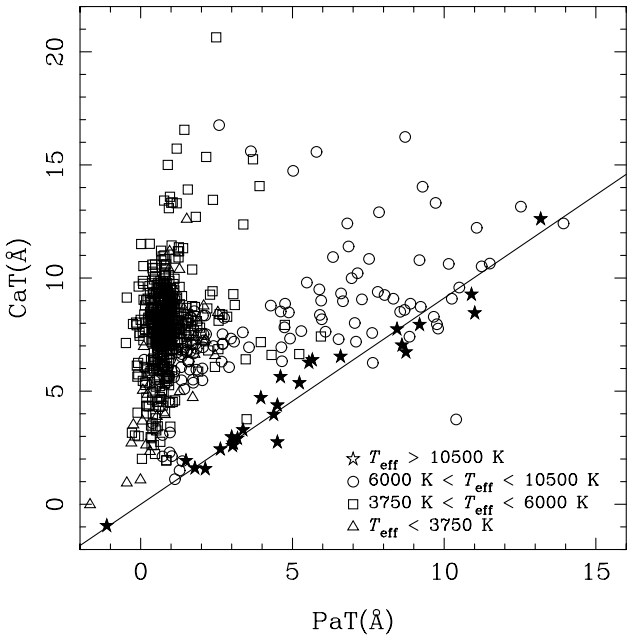

Figure 4. CaT–PaT diagram for the whole stellar library. Different symbols are used to indicate different ranges of effective temperature, as shown in the key. The solid line CaT = 0.93 PaT represents an error weighted least-squares fit to the 26 filled symbols.

Table 5. Ratio between the relative random error of any index and that of CaT.

$\mathcal{I}_{\rm a}$	$\frac{\sigma[\mathcal{I}_{\rm a}]/\mathcal{I}_{\rm a}}{\sigma({\rm CaT})/{\rm CaT}}$
CaT(ZHO)	0.788 ± 0.004
CaT(D&H)	1.009 ± 0.006
CaT(JAJ)	3.938 ± 0.046
CaT(DTT)	0.933 ± 0.007
CaT(A&Z)	0.567 ± 0.002

the S/N ratio per angstrom of the form

$$\sigma[\mathcal{I}_{\rm a}] \simeq \frac{c_1 - c_2\mathcal{I}_{\rm a}}{\rm SN(\AA)}. \quad (5)$$

The exact values of the c_i coefficients are given in equation (A37). As an illustration, for an M0 giant, a S/N per angstrom of 16 is required to measure the CaT and CaT* indices with a 10 per cent uncertainty. We have selected this spectral type since, as we will see in Paper IV, old stellar populations exhibit near-IR spectra close to those or early-M stars.

To compare the sensitivity of our indices to the S/N ratio with that of previous definitions, we have computed the typical random error as a result of photon noise ($\sigma[\mathcal{I}_{\rm a}]$) for the 706 spectra of the library and all the considered index definitions. Table 5 lists the ratio between the relative random error of any index and that of CaT. The relations were computed through a least-squares linear fit (rejecting data outside the 99.73 per cent confidence level) to the relative errors of the whole sample. It can be seen that our index is similar to that of D&H, but leads to somewhat larger random errors than the definitions of ZHO, A&Z and DTT. The reason for this is that these systems use relative narrow central bandpasses (with a total width for the Ca2 and Ca3 lines of 38, 40 and 60 Å respectively, compared to the 80 Å in our definition). Note that since the noise in the bottom of any absorption line is lower than in the wings, indices with narrow central bandpasses yield small random errors. Unfortunately, this turns into a high sensitivity to velocity dispersion broadening (as we will see in Section 4.4.2). On the other hand, the index from JAJ uses a wide central band and extremely narrow continuum bandpasses which increase the uncertainties in the determination of the continuum level. This is why this index shows a high sensitivity to the S/N ratio.

Table 6. Coefficients of the broadening correction polynomials ($\Delta\mathcal{I}_{\rm a}/\mathcal{I}_{\rm a} = a + b\sigma + c\sigma^2 + d\sigma^3$) for the new indices and different spectral types.

$\mathcal{I}_{\rm a}$	Spectral type	$a(\times10^{-3})$	$b(\times10^{-5})$	$c(\times10^{-7})$	$d(\times10^{-9})$
CaT*	F7	0.784	−4.683	6.197	−4.563
	G3	−0.452	1.048	5.386	−4.201
	K0	−1.565	5.605	7.483	−4.418
	M0	−6.240	27.524	3.468	−3.797
	M5	−6.795	27.980	12.715	−3.986
CaT	A0	5.562	−23.662	−4.621	−7.408
	F7	0.503	−2.119	0.559	−5.523
	G3	−1.969	10.305	−5.495	−4.407
	K0	−3.106	15.413	−5.453	−4.332
	M0	−8.542	41.116	−11.118	−3.485
	M5	−3.953	17.938	0.243	−3.751
PaT	A0	3.943	−16.146	−6.162	−4.991
	F7	2.169	−7.226	−10.861	−2.664

As it was also noted in Section 4.2, some Ca indices have been defined as the sum of the two strongest Ca II lines in order to increase the S/N ratio of the final measurement. In our case, when the Ca1 line is removed from the CaT definition, the relative random errors decrease by a factor of 10 per cent. However, keeping in mind that the central bandpass of the Ca3 line falls near the region of strong telluric absorptions, being completely immersed in it for galaxies with $z > 0.03$, we have decided to include the bluest line of the triplet (Ca1) in the index definition, at the expense of sacrificing the gain in accuracy, to ensure a more reliable index measurement for galaxies with relatively high radial velocities.

4.4.2 *Spectral resolution and velocity dispersion broadening*

In order to study the sensitivity of the Ca indices to the spectral resolution or velocity dispersion (σ), we selected a subsample of near-solar metallicity templates of all the spectral types and luminosity classes and broadened their spectra with additional σs from $\sigma = 25$ up to $\sigma = 400\,{\rm km\,s^{-1}}$ (in steps of $25\,{\rm km\,s^{-1}}$). The indices were measured in the full set of broadened spectra, and we computed, for each group of templates with the same spectral type, a third-order polynomial fit to the relative changes of the index values as a function of velocity dispersion

$$\frac{\mathcal{I}_{\rm a}(\sigma) - \mathcal{I}_{\rm a}(\sigma_0)}{\mathcal{I}_{\rm a}(\sigma)} = a + b\sigma + c\sigma^2 + d\sigma^3 \equiv p(\sigma), \quad (6)$$

where $\sigma_0 = 22.2\,{\rm km\,s^{-1}}$, corresponding to the final spectral resolution of the stellar library (FWHM = 1.50Å, see Section 5.2). For a given spectral type, we did not compute separate fits for the different luminosity classes since the derived polynomials were very similar. Using the above equation, it is easy to show that the indices measured at two different velocity dispersions, σ_1 and σ_2, are related by

$$\mathcal{I}_{\rm a}(\sigma_2) = \mathcal{I}_{\rm a}(\sigma_1)\frac{1 - p(\sigma_1)}{1 - p(\sigma_2)}. \quad (7)$$

Table 6 lists the derived coefficients for CaT*, CaT and PaT

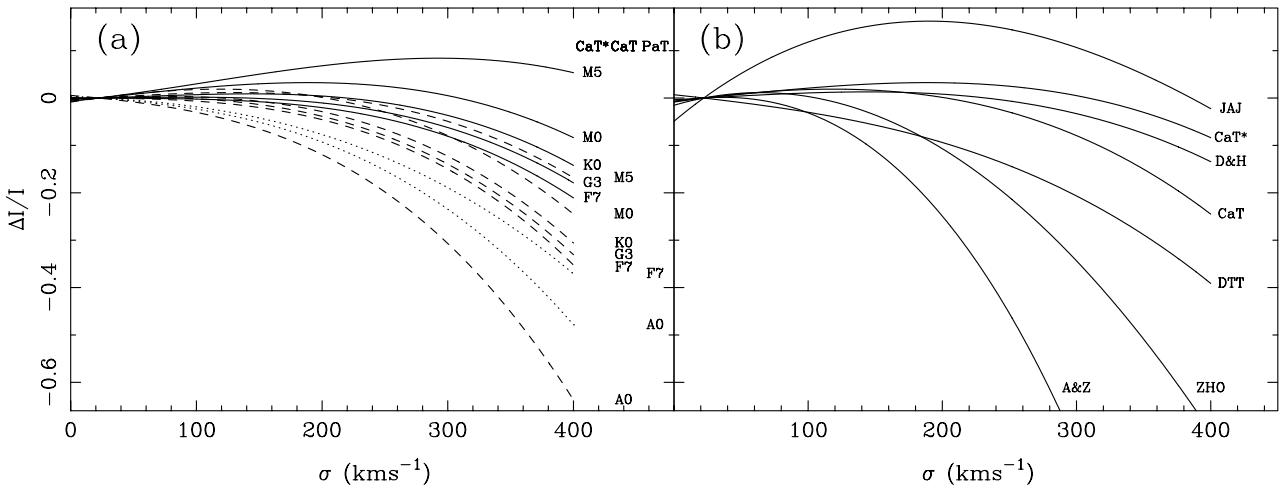

Figure 5. Index sensitivity to the spectral resolution or velocity dispersion broadening. Fig. 5a shows the relative variation of CaT* (solid lines), CaT (dashed lines) and PaT (dotted lines) for several broadened spectral types. In Fig. 5b, similar polynomials are shown for the new and the previous Ca II indices for an M0 type star. In both diagrams, $\Delta I/I$ is zero for $\sigma = 22.2\,\mathrm{km\,s^{-1}}$ (see equation 6), corresponding to the spectral resolution of the stellar library (FWHM = 1.50Å).

Table 7. Coefficients of the broadening correction polynomials ($\Delta\mathcal{I}_a/\mathcal{I}_a = a + b\sigma + c\sigma^2 + d\sigma^3$) for previous index definitions and an M0 spectral type.

$\mathcal{I}_a$	$a(\times10^{-3})$	$b(\times10^{-5})$	$c(\times10^{-7})$	$d(\times10^{-9})$
CaT(A&Z)	−7.712	48.585	−59.578	−12.551
CaT(D&H)	−3.517	15.486	2.396	−3.610
CaT(DTT)	7.107	−31.378	−2.028	−3.755
CaT(JAJ)	−49.068	237.304	−74.233	4.143
CaT(ZHO)	−15.283	83.299	−65.193	0.314

measured over different spectral types. Note that we only provide calibrations for spectral types with equivalent widths significantly different from zero (e.g. stars cooler and hotter than mid-F types for CaT* and PaT, respectively). For illustration, such polynomials are shown in Fig. 5a. It is readily observed that the sensitivity of CaT* to the velocity dispersion broadening is much lower than that of CaT and PaT. Such an improvement is explained since the effects of the broadening on CaT and PaT are partially compensated when the CaT* index is computed. This fact should be considered as another additional advantage of employing generic indices for the measurement of spectral features.

The measurements and fitting procedures given above were also performed for all the previous Ca II indices, although only the calibrations computed for M0 type spectra (see Section 4.4.1) are presented in this paper. The derived coefficients are presented in Table 7, whilst the polynomials, together with those of CaT and CaT* are shown in Fig. 5b. It is clear that, except for the index by D&H, all the previous indices are more sensitive to broadening than our definitions. In most cases, the high sensitivity is a result of the relatively narrow central bandpasses (A&Z; ZHO; DTT). The index by JAJ has wide central bandpasses, but the blue continuum band is located too close to the Ca3 line. Finally, the index by D&H, with wide continuum and central bandpasses, is the only one which overcomes the sensitivity to broadening of CaT, with a similar behaviour to our CaT* index.

4.4.3 Flux calibration

There is no simple recipe to estimate the sensitivity of an index to the uncertainties in the relative flux calibration, since it not only depends on the index definition but also on the response curve of the instrumental configuration. In general, the effect is larger as the wavelength coverage of the sidebands increases. As an illustration, for the JKT runs, the systematic differences between the CaT index measured after and before the flux calibration were around $\Delta\mathrm{CaT} = 0.4$Å. This value is higher than the typical uncertainties because of random errors and any other systematic effects (as we will see in Section 5), and stresses the importance of an accurate flux calibration before performing any meaningful comparison between evolutionary synthesis model predictions and measured spectra.

4.4.4 Sky subtraction

One of the major problems to face in the measurement of spectral features in the near-IR is the presence of both, emission lines produced by the OH radical (e.g. Rousselot et al. 2000), and telluric absorptions arising from water vapour and other molecules (e.g. Stevenson 1994, Chmielewski 2000). A proper removal of these effects heavily relies on the absence of systematic errors in the data reduction. For instance, biases in wavelength calibration (even small sampling aliasing) and in flux calibration (improper flat-fielding, residual fringing, and variable slit width along the slit, among others) seriously compromise an appropriate sky subtraction. These problems can be specially severe when observing faint sources, where the systematic deviations produced by an improper sky subtraction likely exceed random errors. Since the actual relevance of the mentioned uncertainties is a function of many variables, including the radial velocity of the targets, a case by case analysis must be performed to cope with them. Note, however, that the availability of error frames (in which pixels at the position of sky emission lines have larger errors) together with the use of error weighted least-squares fits to determine the pseudo-continuum (see Section 4.3) alleviate the effects of sky residuals in the measurement of generic indices.

4.5 Conversions between different Ca index systems

In this section we give a set of calibrations to make conversions between the different systems of Ca indices. These will be useful

for readers interested in using our system or in transforming their own Ca index data into the new indices.

First, we have compared the measurements of the previous Ca index definitions over the 706 library stars with the corresponding CaT values. The calibrations were computed by deriving an error weighted least-squares fit to a straight line. If the slope of such a fit was not significantly different from 1, we fitted a constant offset. If this term was not significant, we kept the one-to-one relation. Due to the locations of the sidebands of some previous definitions (see Section 4.2), hot and cold stars may depart from the general trend of the rest of the library stars. When this occurs, and in order to ensure the quality of the fit, we have restricted the range of the calibration excluding from the fit those stars with extreme temperatures. In particular, hot stars have not been used for the comparison with A&Z, DTT, ZHO and D&H, where the indices were underestimated as a result of low continuum levels. Similarly, the high continuum levels derived for the cold stars in the systems by JAJ and DTT lead to unreliable indices. Moreover, stars within

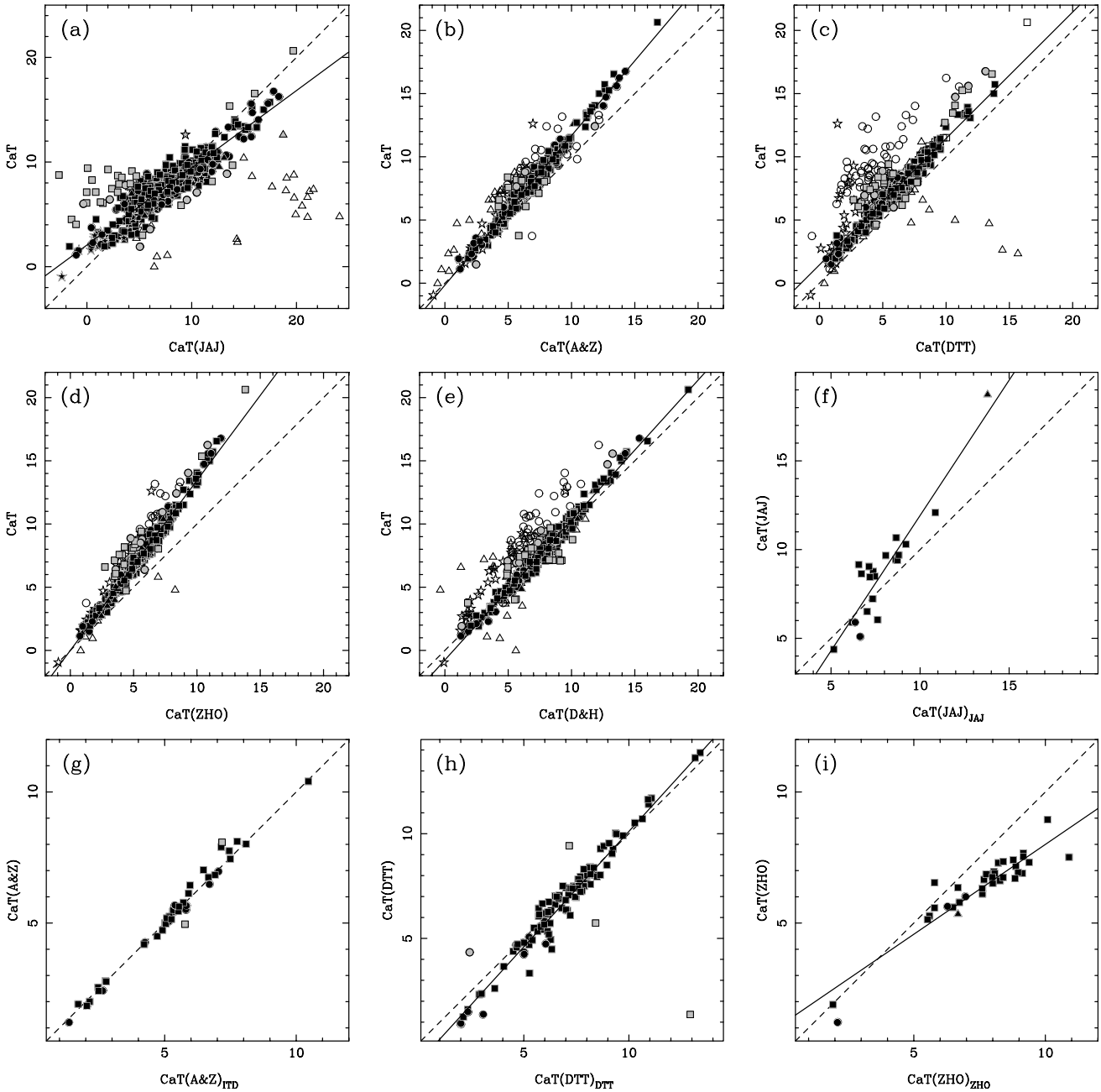

Figure 6. Comparison between different systems. Diagrams (a)–(e) compare the CaT index with the previous indices measured over the 706 stars of the stellar library. CaT(i) means the index in the system by i measured over our spectra. Diagrams (f)–(i) compare measurements of the same index in our and other spectra for a subsample of stars in common. CaT(i)$_j$ means the index in the system by i as measured by j. Label codes are JAJ (Jones et al. 1984), A&Z (Armandroff & Zinn 1988), DTT (Díaz et al. 1989), ZHO (Zhou 1991), D&H (Delisle & Hardy 1992) and ITD (Idiart, Thevenin & de Freitas Pacheco 1997). Symbol types, indicating different ranges of effective temperature, are the same as in Fig. 4. The dashed line shows the one-to-one relation. Grey symbols are stars deviating more than 3σ from the fitted relation, whereas open symbols refer to those stars with effective temperatures outside the fitted range. The solid line marks the most significant fit to the symbols in black. In all the cases, indices are measured in angstrom.

Table 8. Calibrations between different Ca index systems. CaT: New Ca index defined in this paper. CaT(i): Calcium index in the system by i measured in our spectra. CaT(i)$_j$: Calcium index in the system by i as measured in the spectra by j. Codes: JAJ (Jones et al. 1984), A&Z (Armandroff & Zinn 1988), DTT (Díaz et al. 1989), ZHO (Zhou 1991), D&H (Delisle & Hardy 1992) and ITD (Idiart, Thevenin & de Freitas Pacheco 1997). σ: unbiased standard deviation of the fit. N: Number of stars. Range: Effective temperature region where the calibration was obtained.

Calibrations	σ	N	$T_{\rm eff}$ range (K)
CaT = 2.064+0.738 CaT(JAJ)	0.86	627	3600–38400
CaT = −0.155+1.183 CaT(A&Z)	0.34	582	3600–7500
CaT = 1.450+1.000 CaT(DTT)	0.39	486	4000–6300
CaT = 0.002+1.345 CaT(ZHO)	0.35	591	3000–7500
CaT = −0.756+1.107 CaT(D&H)	0.36	559	3600–7000
CaT(JAJ) = −3.322+1.524 CaT(JAJ)$_{\rm JAJ}$	1.15	21	3600–6500
CaT(A&Z) = 0.000+1.000 CaT(A&Z)$_{\rm ITD}$	0.23	41	4350–6300
CaT(DTT) = −0.917+1.103 CaT(DTT)$_{\rm DTT}$	0.55	102	3425–6800
CaT(ZHO) = 1.746+0.616 CaT(ZHO)$_{\rm ZHO}$	0.66	36	3350–6250

the $T_{\rm eff}$ range but deviating by more than 3σ from the fitted relation were also rejected. Most of them are cluster stars with low S/N ratios which present high uncertainties in their Ca measurements. This becomes specially significant in the comparison with JAJ, whose index degrades rapidly as the S/N ratio decreases, producing the large dispersion in the fitted relation. Figs 6a–6e show the calibrations explained above, including the fitted and rejected points and the final fit. CaT(i) refers to the index defined by the reference i measured on our spectra.

Further calibrations are also presented for those papers which measure a Ca index over a sample of stars in common with our stellar library. Following the same procedure to compute the fit, the published index values for the stars in common were compared with the ones obtained by measuring their index over the same stars in our stellar library. It must be noted that, since the measured index is the same in these comparisons, systematic differences between the two sets of measurements are mainly because of flux calibration effects (some authors did not perform any flux calibration) and differences in spectral resolution (although, given the previous resolutions, see Table 1, this is not the dominant effect). The importance of such effects are shown in Figs 6f–6i, where CaT(i)$_j$ now refers to the index defined by i and measured by j.

In Table 8 we present the derived calibrations together with other details of the fits. These fits can be useful for those readers who want to convert their data of previous Ca indices into the new CaT system. The upper calibrations in Table 8 should only be applied once the spectra are on the same spectrophotometric system (i.e. equally flux calibrated) and spectral resolution as the sample of this work. If that is not the case, calibrations like the lower ones in Table 8 should be applied before.

Readers interested in using our Ca system to make comparison of observed line-strengths with the fitting-function predictions that will be presented in the upcoming papers of this series, are highly recommend to convert their observations to this system by:

(i) flux calibrating the spectra,

(ii) observing a significant sample of stars in common with our stellar library,

(iii) converting to our spectral resolution using the relations given in Section 4.4.2 and those that will appear in Paper IV for the integrated spectra of galaxies.

5 COMPUTATION OF THE INDEX ERRORS

One of the principal objectives of this series is to obtain a functional representation of the behaviour of the Ca triplet as a function of the atmospheric stellar parameters (see Paper III). In order to ensure the precision of the final fitting functions, an accurate treatment of the errors is needed. To do this, two kind of error sources must be considered: the uncertainties in the atmospheric parameters (which are thoroughly discussed in Paper II) and those associated with the index measurements, which are the subject of this section.

Following the error analysis described in Gorgas et al. (1999), we divide the error sources into random errors and systematic effects. In brief, the accuracy of the derived random errors will be checked by the comparison of stars with repeated observations within the same run, whereas the systematic errors will be mainly derived by comparisons of stars in common between different runs.

5.1 Random errors

We consider three principal sources of random errors: photon statistics, flux calibration and the combined effect of wavelength calibration and radial velocity uncertainties. Therefore, expected random errors for the ith star can be computed through the following quadratic addition:

$$\sigma^2[\mathcal{I}_{\rm a}]_{{\rm expected},i} = \sigma^2[\mathcal{I}_{\rm a}]_{{\rm photon},i} + \sigma^2[\mathcal{I}_{\rm a}]_{{\rm flux},i} + \sigma^2[\mathcal{I}_{\rm a}]_{{\rm wavelength},i}, \quad (8)$$

where $\mathcal{I}_{\rm a}$ refers to any of the indices.

However, unknown sources of random errors may be present in the data. Following the method described by González (1993), we checked whether the standard deviation of index measurements of stars with multiple observations within the same run was significantly larger than the expected error, $\sigma[\mathcal{I}_{\rm a}]_{\rm expected}$, for the whole run (using a F-test of variances with a significance level of $\alpha = 0.1$). When this occurs, a residual random error $\sigma[\mathcal{I}_{\rm a}]_{\rm residual(1)}$ was derived and introduced in the final random error of each star, $\sigma[\mathcal{I}_{\rm a}]_{{\rm random},i}$, through a multiplicative factor f

$$\sigma[\mathcal{I}_{\rm a}]_{{\rm random},i} = f\,\sigma[\mathcal{I}_{\rm a}]_{{\rm expected},i}, \quad (9)$$

which can be computed as

$$f \simeq \sqrt{1 + \frac{\sigma^2[\mathcal{I}_{\rm a}]_{\rm residual(1)}}{\sigma^2[\mathcal{I}_{\rm a}]_{\rm expected}}}, \quad (10)$$

(see Appendix B for a detailed justification of the above equations). The multiplicative factor for each run was computed by using the index CaT. It was only statistically significant for some runs, being always $f < 1.7$. In particular, run 2 showed an exceptional agreement between the expected and measured CaT errors and no correction was applied.

In the following, a detailed description of the mentioned sources of random errors is given:

(i) Photon statistics and read-out noise. With the aim of tracing the propagation of photon statistics and read-out noise, we followed a parallel reduction of data and error frames with the reduction package R$_{\rm E}$D$^{\rm uc}_{\rm m}$E, which creates error frames at the beginning of the reduction procedure and translates into them, by following the law of combination of errors, all the manipulations performed over the data frames. In this way, the most problematic

reduction steps (flat-field and distortion corrections, wavelength calibration, sky subtraction, etc) are taken into account and, finally, each data spectrum has its corresponding error spectrum which can be used to derive reliable photon errors in the index, $\sigma[\mathcal{I}_a]_{photon}$. Typical errors for the whole sample of stars arising from photon noise are $\sigma[CaT^*]_{photon} = 0.158$, $\sigma[CaT]_{photon} = 0.222$ and $\sigma[PaT]_{photon} = 0.140$. A detailed description of the estimation of random errors in the measurement of classical line-strength indices is shown by CGCG, whereas an analogous treatment for the new generic indices defined in this paper is given in Appendix A2. More details concerning the sensitivity of different indices to the S/N ratio have already been explained in Section 4.4.

(ii) Flux calibration. During each observing night, we observed a sample of spectrophotometric standard stars (from Oke 1990) and derived a flux calibration curve for each one of them. Within the same run, the indices were measured using a final flux calibration curve which was computed by averaging all the individual ones. In addition, we used the individual curves to estimate the random error in the flux calibration as the rms scatter among the different index values obtained with each one of them. Such an error depends on the observing run, but typical values introduced by this effect are $\sigma[CaT^*]_{flux} = 0.033$, $\sigma[CaT]_{flux} = 0.059$ and $\sigma[PaT]_{flux} = 0.057$, being almost negligible in comparison with the photon errors.

(iii) Wavelength calibration and radial velocity. The combined effect of wavelength calibration and radial velocity correction is another random error source. Radial velocities for Coma, Hyades and field stars were taken from the Bibliography of Stellar Radial Velocities (Abt & Biggs 1972) and from the Hipparcos Input Catalogue (Turon et al. 1992), the latter giving mean probable errors of $\sim 5\,km\,s^{-1}$. The adopted values for the cluster stars were the averaged cluster radial velocities: M3, M5, M10, M13, M71, M92 and NGC6171 were taken from Hesser, Shawl & Meyer (1986), NGC188 from Friel (1989), and M67 and NGC7789 from Friel & Janes (1993). Typical radial velocity errors for the cluster stars are $\simeq 15\,km\,s^{-1}$ (~ 0.43 Å at $\lambda 8600$). Once the wavelength calibration procedure was applied to the whole star sample, we still found small shifts (a typical value is 0.32 pixels – or $9.5\,km\,s^{-1}$ – for the JKT runs) between spectra within the same run, and also systematic offsets (an averaged value is 0.51 pixels) between different runs. The deviations within each run were probably because of uncertainties in the published radial velocities and random locations of the star across the spectrograph slit, along the spectral direction. In order to correct for these effects, we cross-correlated each library star with an accurately calibrated reference spectrum (a hot or cool library star depending on the spectral type of the problem spectrum). The derived shifts were applied to the corresponding spectra obtaining thus a highly homogeneous wavelength scale for the whole stellar library. In spite of that, the indices were measured assuming a radial velocity error of $5\,km\,s^{-1}$ which translates into rather small errors, typically $\sigma[CaT^*]_{wavelength} = 0.003$, $\sigma[CaT]_{wavelength} = 0.015$ and $\sigma[PaT]_{wavelength} = 0.003$.

To summarize, photon noise is the main source of random error in the measurement of the present Ca indices. Note, however, that systematic effects such as an improper flux calibration (see Section 4.4.3) can be the dominant source of uncertainty.

5.2 Systematic effects

The main sources of systematic effects in the measurement of spectral indices are spectral resolution, sky subtraction and flux calibration.

(i) Spectral resolution. As is shown in Section 4.4, the new indices are quite insensitive to broadening within an ample range of FWHM values. However, in order to obtain a homogeneous spectral library for stellar population synthesis models, we broadened the spectra in runs 1, 3 and 4 to the spectral resolution of run 2 (1.50 Å). Only the cluster stars corresponding to runs 5 and 6 (12 and 15 stars, respectively) were not broadened. These stars keep the spectral resolution given in Table 2.

(ii) Sky subtraction. The exposure times of most of the library stars are short enough to neglect the effect of an uncertain determination of the sky level. However, some faint cluster stars needed up to 1800 s of exposing time, and many of those in globular clusters were observed with the unavoidable presence of cluster members inside the spectrograph slit which complicated the determination of the sky regions. Although there is not a simple recipe to compute the relevance of this systematic effect, we are confident that the sky subtraction is roughly correct since we do not detect unremoved sky lines. In any case, we have implicitly quantified the sky subtraction uncertainties, as well as that of all the remaining untreated systematic effects, by comparing the amplitude of the final random errors of the same stars in different runs. This procedure is explained in greater detail below (Section 5.3).

(iii) Flux calibration. Systematic errors are expected to be present because of possible differences between the spectrophotometric system of each run. In order to guarantee that all the spectra are in a homogeneous system, we selected run 1 as our spectrophotometric reference system (since it contains a large number of stars in common with other runs) and derived a re-calibration curve for every other run by averaging the ones obtained from stars in common with run 1. Even so, it is not completely sure that our data are in the true spectrophotometric system, so we encourage readers interested in using our results to include in their observing plan stars in common with our stellar sample in order to ensure a proper correction of the data.

5.3 Final errors

In order to check that the systematic effects between runs have been fully corrected, we have compared the Ca indices for the stars in common in the three runs at the JKT applying a *t*-test (see Fig. 7). It is apparent that the agreement between runs is satisfactory.

A new test to improve the random errors derived in Section 5.1 is to compare the index measurements of stars in common between different runs. Considering again run 1 as our reference system, the rest of the runs were compared with it to prove the reliability of the previously derived random errors. If the rms from the index comparison agreed with the expected error obtained from their $\sigma[CaT]_{random,i}$ values (using again an *F*-test of variances), the run being considered was added to the reference system enlarging the fully calibrated set for the following comparison. If this was not the case, we proceeded as in Section 5.1 and a second residual error $\sigma[CaT]_{residual(2)}$ was derived and introduced to the total random error of each star

$$\sigma[CaT]_i = g\sigma[CaT]_{random,i}, \tag{11}$$

where g is now computed as

$$g \simeq \sqrt{1 + \frac{\sigma^2[CaT]_{residual(2)}}{\sigma^2[CaT]_{expected}}}. \tag{12}$$

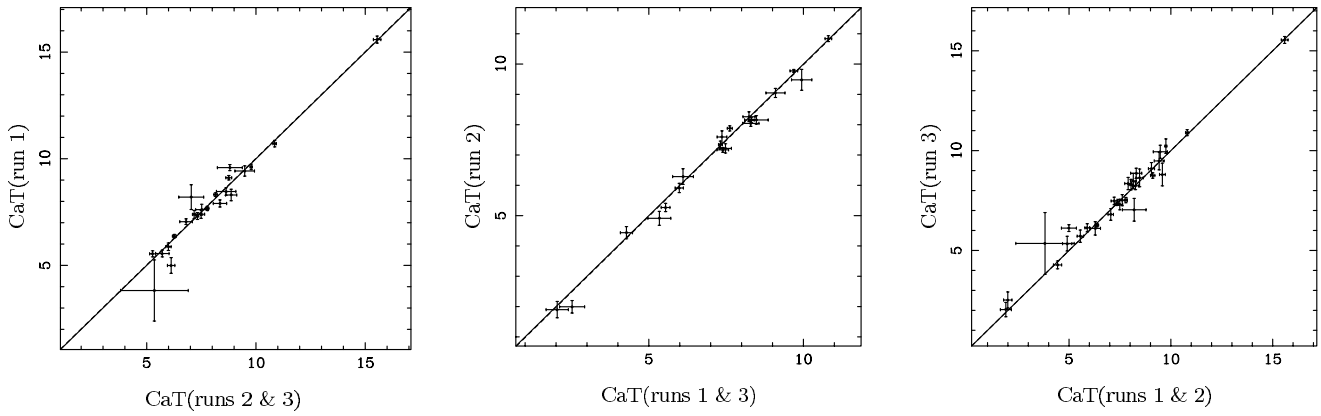

Figure 7. Comparison of the CaT measurements of stars with observations in the JKT runs (1, 2 and 3). The solid line shows the error weighted derived offset, whereas the dashed line (almost hidden by the former fit) displays the one-to-one relation. Error bars for each point are also plotted.

Each time the problem run required a g factor, the whole comparison procedure was repeated. Fortunately, that was only the case of run 6 ($g = 1.65$) which converged in one iteration, and no additional corrections were needed for the other runs.

6 FINAL INDICES AND THE SPECTRAL DATA BASE

After converting the spectra to the same resolution and wavelength scale, final spectra for the repeated stars were obtained through an error-weighted sum of the individual spectra. An electronic data base containing the final spectra of the 706 stars of the stellar library is available at the URL addresses: http://www.ucm.es/info/Astrof/ellipt/CATRIPLET.html and http://www.nottingham.ac.uk/~ppzrfp/CATRIPLET.html.

To summarize, the spectral library spans the range from 8348.85 to 9019.50 Å with a spectral resolution of 1.50 Å (FWHM) although a few cluster stars from runs 5 and 6 keep the original FWHM given in Table 2. The above web page also provides an electronic table listing full information for each star. It includes the indices CaT*, CaT and PaT measured over the final spectra as well as their corresponding errors. The Henry Draper Catalogue number, other names (mainly HR and BD numbers), coordinates (RA and Dec), spectral type, luminosity class, apparent magnitude and atmospheric parameters (that will be derived in Paper II) are also given. This electronic table is also available at the CDS via `http://cdsweb.u-strasbg.fr/Cats.html`.

7 SUMMARY

We present a new stellar library in the near-IR spectral region covering the range λλ8348–9020 at a spectral resolution of 1.5 Å. It consists of 706 stars with atmospheric parameters in the range $2750 < T_{\rm eff} < 38400$ K, $0.00 < \log g < 5.12$ dex, and $-3.45 <$ [Fe/H] $< +0.60$ dex (see Paper II). The aim of this library is to obtain an accurate empirical calibration of the behaviour of the Ca II triplet in individual stars (see the derived fitting functions in Paper III), as well as to derive reliable predictions of the Ca strength and spectral energy distribution of stellar populations in a wide range of ages and metallicities (see Paper IV). For this purpose, we have defined a new set of line-strength indices, namely CaT*, CaT and PaT, which overcome some of the limitations of previous Ca index definitions in this spectral range. In particular, the CaT* index is specially suited to remove the contamination from Paschen lines in the integrated spectra of galaxies. Also, the different sources of random and systematic index errors in these and previous indices have been analysed in detail.

In Section 4.5 we give some recipes for those readers interested in using our system or in converting their own Ca index data into the new CaT indices. Final spectra for the 706 stars of the stellar library and an electronic table listing the index measurements, errors and any other information for each star are available at the web pages given in Section 6. At the same location we also include a set of subroutines to compute the new indices, together with their random errors.

ACKNOWLEDGMENTS

We thank Guy Worthey for providing us with a list of candidate stars at the beginning of this project. Ayvur Peletier's help is acknowledged with the observations and the web page design. AJC acknowledges the hospitality of the Department of Physics (University of Durham) and the School of Physics and Astronomy (University of Nottingham). We also thank S. Pedraz and A. Gil de Paz for helpful suggestions. The JKT, INT and WHT are operated on the island of La Palma by the Royal Greenwich Observatory at the Observatorio del Roque de los Muchachos of the Instituto de Astrofísica de Canarias. The Calar Alto Observatory is operated jointly by the Max-Planck Institute für Astronomie, Heidelberg, and the Spanish Comisión Nacional de Astronomía. This research has made use of the Simbad data base (operated at CDS, Strasbourg, France), the NASAs Astrophysics Data System Article Service, and the Hipparcos Input Catalogue. AJC acknowledges the Comunidad de Madrid for a Formación de Personal Investigador fellowship. AV acknowledges the support of the PPARC rolling grant 'Extragalactic Astronomy and Cosmology in Durham 1998-2002' and of a British Council grant within the British/Spanish Joint Research Programme (Acciones Integradas). This work was supported by the Spanish Programa Sectorial de Promoción del Conocimiento under grant No. PB96-610.

REFERENCES

Abt H. A., Biggs E. S., 1972, Bibliography of Stellar Radial Velocities, KPNO, Latham Process Corp

Allen L. E., Strom K. M., 1995, AJ, 109, 1379

Alloin D., Bica E., 1989, A&A, 217, 57

Anderson C. M., 1974, ApJ, 190, 585
Andrillat Y., Jaschek C., Jaschek M., 1995, A&AS, 112, 475
Armandroff T. E., Da Costa G. S., 1991, AJ, 101, 1329 (A&D)
Armandroff T. E., Zinn R., 1988, AJ, 96, 92 (A&Z)
Armandroff T. E., Da Costa G. S., Zinn R., 1992, AJ, 104, 164
Bender R., Burstein D., Faber S. M., 1993, ApJ, 411, 153
Bevington P. R., 1969, Data reduction and error analysis for the physical sciences, ESO. McGraw-Hill, New York
Bica E., Alloin D., 1987, A&A, 186, 49 (B&A)
Boroson T. A., Thompson I. B., 1991, AJ, 101, 111
Bouw G. D., 1981, PASP, 93, 45
Bower R. G., Lucey J. R., Ellis R. S., 1992, MNRAS, 254, 601
Buonanno R., Corsi C. E., Pecci F., Richer H. B., Fahlman G. G., 1995, AJ, 109, 650
Burstein D., Faber S. M., Gaskell C. M., Krumm N., 1984, ApJ, 287, 586
Burstein D., Faber S. M., González J. J., 1986, AJ, 91, 1130
Cardiel N., 1999, PhD thesis, Universidad Complutense
Cardiel N., Gorgas J., Cenarro J., González J. J., 1998, A&AS, 127, 597 (CGCG)
Carquillat J. M., Jaschek C., Jaschek M., Ginestet N., 1997, A&AS, 123, 5
Carter D., Visvanathan N., Pickles A. J., 1986, ApJ, 311, 637
Cenarro A. J., Gorgas J., Cardiel N., Pedraz S., Peletier R. F., Vazdekis A., 2001a, MNRAS, 326, 981 (Paper II)
Cenarro A. J., Gorgas J., Cardiel N., Vazdekis A., Peletier R. F., 2001b, MNRAS, submitted (Paper III)
Chmielewski Y., 2000, A&A, 353, 666
Cohen J. G., 1978, ApJ, 221, 788
Cohen J. G., 1979, ApJ, 228, 405
Cole A. A., Smecker-Hane T. A., Gallagher J. S., III, 2000, AJ, 120, 1808
Da Costa G. S., Armandroff T. E., 1995, AJ, 109, 2533
Da Costa G. S., Hatzidimitriou D., 1998, AJ, 115, 1934
Da Costa G. S., Armandroff T. E., Norris J. E., 1992, AJ, 104, 154
Davies R. L., Sadler E. M., Peletier R. F., 1993, MNRAS, 262, 650
Delisle S., Hardy E., 1992, AJ, 103, 711 (D&H)
Dempsey R. C., Bopp B. W., Henry G. W., Hall D. S., 1993, ApJS, 86, 293
Díaz A. I., Terlevich E., Terlevich R., 1989, MNRAS, 239, 325 (DTT)
Erdelyi-Mendes M., Barbuy B., 1991, A&A, 241, 176
Faber S. M., French H. B., 1980, ApJ, 235, 405
Faber S. M., Friel E. D., Burstein D., Gaskell C. M., 1985, ApJS, 57, 711
Faber S. M., Trager S. C., González J. J., Worthey G., 1995, in van der Kruit P. C., Gilmore G., eds, Proc. IAU Symp. 164, Stellar Populations. Kluwer, Dordrecht, p. 249
Fluks M. A., Plez B., Thé P. S., de Winter D., Westerlund B. E., Steenman H. C., 1994, A&AS, 105, 311
Forbes D. A., Boisson C., Ward M. J., 1992, MNRAS, 259, 293
Friel E. D., 1989, PASP, 101, 244
Friel E. D., Janes K. A., 1993, A&A, 267, 75
Gallagher J. S., III, Smith L. J., 1999, MNRAS, 304, 540
García-Vargas M. L., Díaz A. I., Terlevich E., Terlevich R., 1993, Ap&SS, 205, 85
García Vargas M. L., González Delgado R. M., Pérez E., Alloin D., Díaz A. I., Terlevich E., 1997, ApJ, 478, 112
García Vargas M. L., Mollá M., Bressan A., 1998, A&AS, 130, 513
Garzón F., López-Corredoira M., Hammersley P., Mahoney T. J., Calbet X., Beckman J. E., 1997, ApJ, 491, L31
Geisler D., 1984, PASP, 96, 723
Geisler D., Piatti A. E., Clariá J. J., Minniti D., 1995, AJ, 109, 605
Ginestet N., Carquillat J. M., Jaschek M., Jaschek C., 1994, A&AS, 108, 359
González J. J., 1993, PhD thesis, Univ. California
González J. J., Gorgas J., 1996, in Buzzoni A., Renzini A., Serrano A., eds, ASP Conf. Ser. Vol. 86, Fresh Views of Elliptical Galaxies. Astron. Soc. Pac., San Francisco, p. 225
González Delgado R. M., Pérez E., 1996a, MNRAS, 278, 737
González Delgado R. M., Pérez E., 1996b, MNRAS, 280, 53
González Delgado R. M., Leitherer C., Heckman T., Cerviño M., 1997, ApJ, 483, 705
Gorgas J., Efstathiou G., Aragón-Salamanca A., 1990, MNRAS, 245, 217
Gorgas J., Faber S. M., Burstein D., González J. J., Courteau S., Prosser C., 1993, ApJS, 86, 153
Gorgas J., Cardiel N., Pedraz S., González J. J., 1999, A&AS, 139, 29
Goudfrooij P., Mack J., Kissler-Pattig M., Meylan G., Minniti D., 2001, MNRAS, 322, 643
Heckman T. M., González Delgado R., Leitherer C., Meurer G. R., Krolik J., Wilson A. S., Koratkar A., Kinney A., 1997, ApJ, 482, 114
Hesser J. E., Shawl S. J., Meyer J. E., 1986, PASP, 98, 403
Houdashelt M. L., 1995, PhD thesisThe Ohio State Univ.
Humphreys R. M., Pennington R. L., Jones T. J., Ghigo F. D., 1988, AJ, 96, 1884
Idiart T. P., Thévenin F., de Freitas Pacheco J. A., 1997, AJ, 113, 1066 (ITD)
Jones L. A., 1997, PhD thesis, Univ. North Carolina
Jones L. A., Worthey G., 1995, ApJ, 446, L31
Jones J. E., Alloin D. M., Jones B. J. T., 1984, ApJ, 283, 457 (JAJ)
Jørgensen I., 1999, MNRAS, 306, 607
Jørgensen U. G., Carlsson M., Johnson H. R., 1992, A&A, 254, 258
Keenan P. C., Hynek J. A., 1945, ApJ, 101, 265
Kirkpatrick J. D., Henry T. J., McCarthy D. W., 1991, ApJS, 77, 417
Kuntschner H., 2000, MNRAS, 315, 184
Linsky J. L., Hunten D., Glacken D., Kelch W., 1979, ApJS, 41, 481
Mallik S. V., 1994, A&AS, 103, 279
Mallik S. V., 1997, A&AS, 124, 359
Mantegazza L., 1992, A&A, 265, 527
Massey P., 1998, ApJ, 501, 153
Mayya Y. D., 1997, ApJ, 482, L149
Merrill P. W., 1934, ApJ, 79, 183
Molla M., García-Vargas M. L., 2000, A&A, 359, 18
Montes D., Martín E. L., 1998, A&AS, 128, 485
Montes D., Sanz-Forcada J., Fernández-Figueroa M. J., De Castro E., Poncet A., 1998, A&A, 330, 155
Montes D., Ramsey L. W., Welty A. D., 1999, ApJS, 123, 283
Munari U., Tomasella L., 1999, A&AS, 137, 521
O'Connell R. W., 1973, AJ, 78, 1074
O'Connell R. W., 1976, ApJ, 206, 370
Oke J. B., 1990, AJ, 99, 1621
Olszewski E. W., Schommer R. A., Suntzeff N. B., Harris H., 1991, AJ, 101, 515
Parsons S. B., 1964, ApJ, 140, 853
Pedraz S., Gorgas J., Cardiel N., Guzmán R., 1999, Ap&SS, 263, 159
Peletier R. F., 1999, in Beckman J. E., Mahoney T. J., eds, ASP Conf. Ser. Vol. 187, The Evolution of Galaxies on Cosmological Timescales. Astron. Soc. Pac., San Francisco, p. 231
Peletier R. F., Vazdekis A., Arribas S., del Burgo C., García-Lorenzo B., Gutiérrez C., Mediavilla E., Prada F., 1999, MNRAS, 310, 863
Pérez E., Márquez I., Marrero I., Durret F., González Delgado R. M., Masegosa J., Maza J., Moles M., 2000, A&A, 353, 893
Ponder J. M. et al., 1998, AJ, 116, 2297
Prada F., Greve A., McKeith C. D., 1994, A&A, 288, 396
Rich R. M., 1988, AJ, 95, 828
Rose J. A., 1994, AJ, 107, 206
Rosenberg A., Piotto G., Saviane I., Aparicio A., Gratton R., 1998, AJ, 115, 658
Rousselot P., Lidman C., Cuby J. G., Moreels G., Monnet G., 2000, A&A, 354, 1134
Rutledge G. A., Hesser J. E., Stetson P. B., Mateo M., Simard L., Bolte M., Friel E. D., Copin Y., 1997a, PASP, 109, 883
Rutledge G. A., Hesser J. E., Stetson P. B., 1997b, PASP, 109, 907 (RHS)
Sánchez-Blázquez P., Gorgas J., Cardiel N., Pedraz S., Cenarro A. J., Bruzual G., 2000, Ap&SS, in press
Savage B. D., Mathis J. S., 1979, ARA&A, 17, 73
Schiavon R. P., Barbuy B., Bruzual G., 2000, ApJ, 532, 453
Serote Roos M., Boisson C., Joly M., 1996, A&AS, 117, 93
Sharpless S., 1956, ApJ, 124, 342
Smecker-Hane T. A., Mandushev G. I., Hesser J. E., Stetson P. B., Da Costa G. S., Hatzidimitriou D., 1999, in Hubeny I., Heap S., Cornett R., eds, ASP Conf. Ser. Vol. 192, Spectro–Photometric Dating of Stars and Galaxies. Astron. Soc. Pac., San Francisco, p. 159

Smith G., Drake J. J., 1987, A&A, 181, 103
Smith G., Drake J. J., 1990, A&A, 231, 125
Spinrad H., Taylor B., 1971, ApJS, 22, 445
Stevenson C. C., 1994, MNRAS, 267, 904
Suntzeff N. B., Kraft R. P., 1996, AJ, 111, 1913
Suntzeff N. B., Schommer R. A., Olszewski E. W., Walker A. R., 1992, AJ, 104, 1743
Suntzeff N. B., Mateo M., Terndrup D. M., Olszewski E. W., Geisler D., Weller W., 1993, ApJ, 418, 208
Terlevich E., Díaz A. I., Terlevich R., 1990a, MNRAS, 242, 271
Terlevich E., Terlevich R., Díaz A. I., Pastoriza M. G., Dottori H., 1990b, MNRAS, 242, 48, P
Terlevich E., Díaz A. I., Terlevich R., González Delgado R. M., Pérez E., García-Vargas M. L., 1996, MNRAS, 279, 1219
Terlevich A., Kuntschner H., Bower R. G., Caldwell N., Sharples R., 1999, MNRAS, 310, 445
Thévenin F., 1998, Bull. Inf. Cent. Données Stellaires, 49, 193
Trager S. C., Faber S. M., Worthey G., González J. J., 2000a, AJ, 119, 1645
Trager S. C., Faber S. M., Worthey G., González J. J., 2000b, AJ, 120, 165
Turon C. et al., 1992, Bull. Inf. Cent. Données Stellaires, 41, 9
Vazdekis A., 1999, ApJ, 513, 224
Vazdekis A., Arimoto N., 1999, ApJ, 525, 144
Vazdekis A., Casuso E., Peletier R. F., Beckman J. E., 1996, ApJS, 106, 307
Vazdekis A., Peletier R. F., Beckman J. E., Casuso E., 1997, ApJS, 111, 203
Wilson O. C., Merrill P. W., 1937, ApJ, 86, 162
Worthey G., 1998, PASP, 110, 888
Worthey G., Ottaviani D. L., 1997, ApJS, 111, 377
Worthey G., Faber S. M., González J. J., Burstein D., 1994, ApJS, 94, 687
Zhou X., 1991, A&A, 248, 367 (ZHO)

APPENDIX A: COMPUTATION OF GENERIC INDICES AND ASSOCIATED RANDOM ERRORS

In this appendix we give full details concerning the definition and practical measure of a new type of line-strength index, which will be referred to as *generic* index. In particular, the new indices defined and introduced in this paper, namely the CaT, PaT and CaT*, are examples of generic indices.

First, we briefly summarize the main properties of classical indices. Their generalization into generic indices appears, in a natural way, when introducing three new requirements in the measure of spectral features. The necessity of such a change is readily justified when we consider the advantages of the new definition. Finally, we face the derivation of approximate formulae for the estimation of random errors from the mean S/N ratio per angstrom.

A1 Classical indices

The aim of the use of line-strength indices is to obtain a quantitative measure of a spectral signature. Up to date, most authors have employed line-strength indices whose definitions are close to the expression of equivalent width,

$$W_\lambda(\mathring{\mathrm{A}}) = \int_{\mathrm{line}} [1 - S(\lambda)/C(\lambda)]\,\mathrm{d}\lambda, \tag{A1}$$

where $S(\lambda)$ corresponds to the observed spectrum, and $C(\lambda)$ is the continuum level at the line location obtained by the interpolation of $S(\lambda)$ in the local continuum. Note that, as it was pointed out by Geisler (1984) (see also Rich 1988), at low spectral resolution a pseudo-continuum is measured instead of a true continuum. In order to prevent subjective determinations of the continuum and absorption regions, *atomic* indices have been established by characterizing each index with the help of three wavelength bandpasses: the relevant spectral feature is covered by the central bandpass, whereas the other two bandpasses, located at both sides of the central region, are employed to define the continuum reference level through a linear interpolation. In particular atomic indices are computed as (using the notation employed by González 1993)

$$I_{\mathrm{a}}(\mathring{\mathrm{A}}) \equiv \int_{\lambda_{c_1}}^{\lambda_{c_2}} [1 - S(\lambda)/C(\lambda)]\,\mathrm{d}\lambda, \tag{A2}$$

where λ_{c_1} and λ_{c_2} are the limits of the central bandpass, $S(\lambda)$ is the observed spectrum, and $C(\lambda)$ is the local pseudo-continuum, which is derived by

$$C(\lambda) \equiv S_b \frac{\lambda_r - \lambda}{\lambda_r - \lambda_b} + S_r \frac{\lambda - \lambda_b}{\lambda_r - \lambda_b}, \tag{A3}$$

where

$$S_b \equiv \frac{\int_{\lambda_{b_1}}^{\lambda_{b_2}} S(\lambda)\,\mathrm{d}\lambda}{(\lambda_{b_2} - \lambda_{b_1})}, \qquad S_r \equiv \frac{\int_{\lambda_{r_1}}^{\lambda_{r_2}} S(\lambda)\,\mathrm{d}\lambda}{(\lambda_{r_2} - \lambda_{r_1})}, \tag{A4}$$

$$\lambda_b \equiv (\lambda_{b_1} + \lambda_{b_2})/2, \qquad \lambda_r \equiv (\lambda_{r_1} + \lambda_{r_2})/2, \tag{A5}$$

λ_{b_1}, λ_{b_2}, λ_{r_1}, and λ_{r_2} being the limits of the blue and red bandpasses, respectively. Following the same philosophy, broader spectral lines and molecular band features are usually measured in magnitudes using the so-called *molecular* indices, which are computed as

$$I_{\mathrm{m}}(\mathrm{mag}) \equiv -2.5 \log_{10}\left(1 - \frac{I_{\mathrm{a}}}{\lambda_{c_2} - \lambda_{c_1}}\right). \tag{A6}$$

The error estimate in atomic and molecular indices was extensively analysed by CGCG (see also Cardiel 1999). These authors derived a set of accurate formulae for the computation of random errors in line-strength indices. The applicability of the error formulae depends on the availability of reliable error spectra. For this purpose, error frames can be created at the beginning of the reduction procedure and processed in parallel with the data frames. In addition, it is possible to use simple expressions to estimate the absolute index errors as a function of the mean S/N ratio per angstrom. In particular, the error of the atomic indices can be derived by

$$\sigma[I_{\mathrm{a}}] \approx \frac{c_1 - c_2 I_{\mathrm{a}}}{\mathrm{SN}(\mathring{\mathrm{A}})}, \tag{A7}$$

whereas for the molecular indices the expression is

$$\sigma[I_{\mathrm{m}}] \approx \frac{2.5 \log_{10} \mathrm{e}\, c_2}{\mathrm{SN}(\mathring{\mathrm{A}})} \approx \frac{1.086\, c_2}{\mathrm{SN}(\mathring{\mathrm{A}})} \approx \frac{c_2}{\mathrm{SN}(\mathring{\mathrm{A}})}, \tag{A8}$$

SN(Å) being the averaged S/N ratio measured in pixels included in the three bandpasses, and c_1 and c_2 two constants which depend on the index definition.

A2 Generic indices

The classical index definition can be generalized by including several spectral features in a single measurement. In particular it is possible to define a generic index which can be characterized by an arbitrary number of continuum and spectral-feature bandpasses. Apart from this modification, we have also considered two additional requirements: the possibility of modifying the contribution of each spectral-feature bandpass (by defining a

multiplicative factor for each spectral feature), and the derivation of the pseudo-continuum using an error weighted least-squares fit.

Taking all the mentioned requirements into account, the generic index can be defined as

$$\mathcal{I}_{\rm a}(\text{Å}) \equiv \sum_{k=1}^{N_{\rm f}} \left\{ \xi(k) \int_{\lambda_{c_1}(k)}^{\lambda_{c_2}(k)} [1 - S(\lambda)/C(\lambda)]\, {\rm d}\lambda \right\}, \tag{A9}$$

where the subscript 'a' indicates that this index is the generalization of the classical atomic index (i.e. it is measured in Å), $N_{\rm f}$ is the number of spectral-feature bandpasses, $\xi(k)$ is the multiplicative factor associated to each of these bandpasses, and $\lambda_{c_1}(k)$ and $\lambda_{c_2}(k)$ are the limits of the kth spectral-feature bandpass. The pseudo-continuum is assumed to be obtained through an error weighted least-squares fit to $N_{\rm c}$ continuum bandpasses.

In practice, the integrals in equation (A9) must be replaced by summations, i.e.

$$\mathcal{I}_{\rm a}(\text{Å}) \simeq \Theta \sum_{k=1}^{N_{\rm f}} \left\{ \xi(k) \sum_{i=1}^{N(k)} [1 - S(\lambda_{k,i})/C(\lambda_{k,i})] \right\}, \tag{A10}$$

where Θ is the linear dispersion (in Å pixel^{-1}, assumed to be constant along the spectrum), $N(k)$ is the number of pixels covering the kth spectral-feature bandpass, and $\lambda_{k,i}$ is the central wavelength of the ith pixel in the kth bandpass. The continuum level is derived as (see e.g. Bevington 1969)

$$C(\lambda_{k,i}) = \alpha_1 + \alpha_2 \lambda_{k,i} \tag{A11}$$

with

$$\alpha_1 = \frac{1}{\Delta}(\Sigma_3\Sigma_4 - \Sigma_2\Sigma_5), \tag{A12}$$

$$\alpha_2 = \frac{1}{\Delta}(\Sigma_1\Sigma_5 - \Sigma_2\Sigma_4), \tag{A13}$$

$$\Delta = \Sigma_1\Sigma_3 - \Sigma_2\Sigma_2, \tag{A14}$$

where we have defined the following parameters

$$\Sigma_1 \equiv \sum_{n=1}^{N_{\rm c}} \sum_{h=1}^{M(n)} \frac{1}{\sigma^2[S(\lambda_{n,h})]}, \tag{A15}$$

$$\Sigma_2 \equiv \sum_{n=1}^{N_{\rm c}} \sum_{h=1}^{M(n)} \frac{\lambda_{n,h}}{\sigma^2[S(\lambda_{n,h})]}, \tag{A16}$$

$$\Sigma_3 \equiv \sum_{n=1}^{N_{\rm c}} \sum_{h=1}^{M(n)} \frac{\lambda_{n,h}^2}{\sigma^2[S(\lambda_{n,h})]}, \tag{A17}$$

$$\Sigma_4 \equiv \sum_{n=1}^{N_{\rm c}} \sum_{h=1}^{M(n)} \frac{S(\lambda_{n,h})}{\sigma^2[S(\lambda_{n,h})]}, \tag{A18}$$

and

$$\Sigma_5 \equiv \sum_{n=1}^{N_{\rm c}} \sum_{h=1}^{M(n)} \frac{\lambda_{n,h} S(\lambda_{n,h})}{\sigma^2[S(\lambda_{n,h})]}, \tag{A19}$$

$M(n)$ being the number of pixels covering the nth continuum bandpass, and $\sigma^2 S(\lambda_{n,h})]$ the variance of the observed spectrum at the central wavelength of the hth pixel in the nth continuum bandpass.

It is important to note that since, in general, the limits of the bandpasses will not be coincident with the wavelengths corresponding to the edges of each pixel, fractions of pixels must be considered when performing the summations at the borders of such bandpasses.

Using the same notation, the generalization of the classical molecular index is straightforward, namely

$$\mathcal{I}_{\rm m}({\rm mag}) \equiv -2.5 \log_{10} \left\{ 1 - \frac{\mathcal{I}_{\rm a}}{\sum_{k=1}^{N_{\rm f}} \xi(k)[\lambda_{c_2}(k) - \lambda_{c_1}(k)]} \right\}, \tag{A20}$$

where the subscript 'm' denotes that this index is measured in magnitudes.

Next, and in order to derive analytical expressions for the computation of random errors in the generic indices, we follow a similar treatment to that described by CGCG for the classical indices. The expected random error in the measurement of a generic index of the form given in equation (A10) can be expressed as

$$\frac{\sigma[\mathcal{I}_{\rm a}]}{\Theta} \simeq \sigma \left[\sum_{k=1}^{N_{\rm f}} \left\{ \xi(k) \sum_{i=1}^{N(k)} [S(\lambda_{k,i})/C(\lambda_{k,i})] \right\} \right], \tag{A21}$$

where the right-hand term is a function of $2 \times \sum_{k=1}^{N_{\rm f}} N(k)$ variables, $(\ldots, S(\lambda_{k,i}), \ldots, C(\lambda_{k,i}), \ldots)$, which are not all independent. In fact, if one assumes that none of the $N_{\rm f} + N_{\rm c}$ spectral-feature and continuum bandpasses overlap, and taking into account that $C(\lambda)$ is a linear fit to $S(\lambda)$ in $N_{\rm c}$ continuum bandpasses, the covariance terms verify

$$\begin{aligned}
&{\rm cov}(S(\lambda_{k,i}), C(\lambda_{m,j})) = 0 \qquad \forall k, m, i, j, \\
&{\rm cov}(C(\lambda_{k,i}), C(\lambda_{m,j})) \neq 0 \qquad \forall k, m, i, j, \\
&{\rm cov}(S(\lambda_{k,i}), S(\lambda_{m,j})) = 0 \qquad \begin{cases} \forall k, m, i, j \\ \text{except for } i = j \text{ when } k = m, \end{cases} \\
&\text{with } \begin{cases} k, m \in [1, N_{\rm f}], \\ i, j \in [1, N(k)]. \end{cases}
\end{aligned} \tag{A22}$$

With these results in mind, and taking partial derivatives in equation (A21), it is easy to obtain

$$\begin{aligned}
&\left(\frac{\sigma[\mathcal{I}_{\rm a}]}{\Theta} \right)^2 \\
&\simeq \sum_{l=1}^{N_{\rm f}} \sum_{i=1}^{N(l)} \left\{ \xi^2(l) \frac{C^2(\lambda_{l,i})\sigma^2[S(\lambda_{l,i})] + S^2(\lambda_{l,i})\sigma^2[C(\lambda_{l,i})]}{C^4(\lambda_{l,i})} \right\} \\
&+ \sum_{l=1}^{N_{\rm f}} \sum_{i=1}^{N(l)} \sum_{\substack{m=1 \\ j \neq i}}^{N_{\rm f}} \sum_{\substack{j=1 \\ \text{when } m=l}}^{N(m)} \\
&\times \left\{ \xi(l)\xi(m) \frac{S(\lambda_{l,i})S(\lambda_{m,j})}{C^2(\lambda_{l,i})C^2(\lambda_{m,j})} {\rm cov}(C(\lambda_{l,i}), C(\lambda_{m,j})) \right\}
\end{aligned} \tag{A23}$$

where $\sigma^2 C(\lambda_{k,i})]$ is the variance of the fitted continuum, evaluated at the ith pixel of the kth spectral-feature bandpass. Remembering that equation (A11) is a function of $3 \times \sum_{n=1}^{N_{\rm c}} M(n)$ variables, $(\ldots, \lambda_{l,r}, \ldots, S(\lambda_{l,r}), \ldots, \sigma_{S(\lambda_{l,r})}, \ldots)$, of which only $[\ldots, S(\lambda_{l,r}), \ldots]$ have error, it is possible to write

$$\sigma^2[C(\lambda_{k,i})] = \sum_{l=1}^{N_{\rm c}} \sum_{r=1}^{M(l)} \left[\frac{\partial C(\lambda_{k,i})}{\partial S(\lambda_{l,r})} \right]^2 \sigma^2[S(\lambda_{l,r})], \tag{A24}$$

with

$$\frac{\partial C(\lambda_{k,i})}{\partial S(\lambda_{l,r})} = \frac{1}{\Delta}\left\{\frac{1}{\sigma^2[S(\lambda_{l,r})]}\Sigma_3 - \frac{\lambda_{l,r}}{\sigma^2[S(\lambda_{l,r})]}\Sigma_2\right\} + \frac{\lambda_{k,i}}{\Delta}\left\{\frac{\lambda_{l,r}}{\sigma^2[S(\lambda_{l,r})]}\Sigma_1 - \frac{1}{\sigma^2[S(\lambda_{l,r})]}\Sigma_2\right\}. \quad \text{(A25)}$$

The non-null covariance terms in equation (A23) can be derived using the definition of covariance

$$\begin{aligned}\mathrm{cov}(C(\lambda_{k,i}), C(\lambda_{m,j})) &= \langle C(\lambda_{k,i})C(\lambda_{m,j})\rangle - \langle C(\lambda_{k,i})\rangle\langle C(\lambda_{m,j})\rangle \\ &= [\langle\alpha_1\alpha_1\rangle - \langle\alpha_1\rangle\langle\alpha_1\rangle] \\ &+ [\langle\alpha_1\alpha_2\rangle - \langle\alpha_1\rangle\langle\alpha_2\rangle](\lambda_{k,i} + \lambda_{m,j}) \\ &+ [\langle\alpha_2\alpha_2\rangle - \langle\alpha_2\rangle\langle\alpha_2\rangle]\lambda_{k,i}\lambda_{m,j}. \quad \text{(A26)}\end{aligned}$$

Using the parameters defined in equations (A15)–(A19), and taking into account that their variances verify

$$\begin{aligned}\sigma^2[\Sigma_1] &= \sigma^2[\Sigma_2] = \sigma^2[\Sigma_3] = 0, \\ \sigma^2[\Sigma_4] &= \Sigma_1, \quad \text{and} \quad \sigma^2[\Sigma_5] = \Sigma_3, \quad \text{(A27)}\end{aligned}$$

is not difficult to show that

$$\langle\alpha_1\alpha_1\rangle - \langle\alpha_1\rangle\langle\alpha_1\rangle = \frac{1}{\Delta^2}[\Sigma_1\Sigma_3\Sigma_3 - \Sigma_2\Sigma_2\Sigma_3], \quad \text{(A28)}$$

$$\langle\alpha_1\alpha_2\rangle - \langle\alpha_1\rangle\langle\alpha_2\rangle = \frac{1}{\Delta^2}[\Sigma_2\Sigma_2\Sigma_2 - \Sigma_1\Sigma_2\Sigma_3], \quad \text{(A29)}$$

$$\langle\alpha_2\alpha_2\rangle - \langle\alpha_2\rangle\langle\alpha_2\rangle = \frac{1}{\Delta^2}[\Sigma_1\Sigma_1\Sigma_3 - \Sigma_1\Sigma_2\Sigma_2]. \quad \text{(A30)}$$

On the other hand, the expected random error in generic indices measured in magnitudes, equation (A20), can be computed with

$$\frac{\sigma[\mathcal{I}_\mathrm{m}]}{\sigma[\mathcal{I}_\mathrm{a}]} = \frac{2.5\log_{10}\mathrm{e}}{10^{-0.4\mathcal{I}_\mathrm{m}}\sum_{k=1}^{N_\mathrm{f}}\{\xi(k)[\lambda_{c_2}(k) - \lambda_{c_1}(k)]\}}. \quad \text{(A31)}$$

We have verified the reliability of the new set of formulae by comparing the measured CaT, PaT and CaT* random errors in the 706 stars of the library, with the errors derived with the help of numerical simulations (see Section 4 in CGCG). This comparison, which is graphically displayed in Fig. A1, indicates that the agreement is complete. Note, however, that the use of analytical formulae instead of numerical simulations should be preferred since the latter constitutes a computer-time demanding method.

When the previous formulae are applied over spectra corresponding to redshifted objects, it is important to remember that generic indices of the form given by equation (A9), and their errors, must be corrected to rest-frame values by

$$\begin{aligned}\mathcal{I}_\mathrm{a}|_{z=0} &= \frac{1}{1+z}\mathcal{I}_\mathrm{a}|_z, \\ \sigma[\mathcal{I}_\mathrm{a}]_{z=0} &= \frac{1}{1+z}\sigma[\mathcal{I}_\mathrm{a}]_z, \quad \text{(A32)}\end{aligned}$$

where $\mathcal{I}_\mathrm{a}|_z$ and $\mathcal{I}_\mathrm{a}|_{z=0}$ are the redshifted and rest-frame indices, $\sigma\mathcal{I}_\mathrm{a}]_z$ and $\sigma[\mathcal{I}_\mathrm{a}]_{z=0}$ are their corresponding errors, and z is the redshift. Generic indices of the form given by equation (A20), in magnitudes, and their errors, do not require correction by redshift.

It is important to note that an appropriate treatment of covariance terms is essential in order to guarantee the accuracy of the error estimate. Neglecting such terms can lead to important systematic anomalies in the determination of random errors. For illustration, we have studied this effect on the generic indices CaT, PaT and CaT*. For this purpose, we measured the individual absorption features of CaT and PaT using a new set of indices, CaT_1, CaT_2 and CaT_3, and PaT_1, PaT_2 and PaT_3, respectively, which were defined as generic indices with the same continuum bandpasses as the CaT and PaT indices. In this way, the CaT, PaT and CaT* are obviously derived as a linear combination of the new set, i.e.

$$\begin{aligned}\mathrm{CaT} &= \mathrm{CaT}_1 + \mathrm{CaT}_2 + \mathrm{CaT}_3, \\ \mathrm{PaT} &= \mathrm{PaT}_1 + \mathrm{PaT}_2 + \mathrm{PaT}_3, \\ \mathrm{CaT}^* &= \mathrm{CaT}_1 + \mathrm{CaT}_2 + \mathrm{CaT}_3 - 0.93(\mathrm{PaT}_1 + \mathrm{PaT}_2 + \mathrm{PaT}_3). \quad \text{(A33)}\end{aligned}$$

Using equation (A23) for the computation of random errors in CaT_i and PaT_i (with $i = 1, 2, 3$) in the 706 stars of the library, and adding errors quadratically neglecting covariance terms in the set CaT_i, PaT_i, leads to

$$\begin{aligned}\sigma[\Sigma_{i=1}^3\mathrm{CaT}_i] &= \left(\sum_{i=1}^3\sigma^2[\mathrm{CaT}_i]\right)^{1/2}, \\ \sigma[\Sigma_{i=1}^3\mathrm{PaT}_i] &= \left(\sum_{i=1}^3\sigma^2[\mathrm{PaT}_i]\right)^{1/2}, \\ \sigma[\Sigma_{i=1}^3\mathrm{CaT}_i - 0.93\Sigma_{i=1}^3\mathrm{PaT}_i] &= \left(\sum_{i=1}^3\sigma^2[\mathrm{CaT}_i] + 0.93^2\sum_{i=1}^3\sigma^2[\mathrm{PaT}_i]\right)^{1/2}. \quad \text{(A34)}\end{aligned}$$

The application of these approximate formulae, in comparison with the accurate expression given in equation (A23), gives

$$\begin{aligned}&\sigma[\Sigma_{i=1}^3\mathrm{CaT}_i]/\sigma[\mathrm{CaT}] = 0.7865, \ \mathrm{rms} = 0.0042, \\ &\sigma[\Sigma_{i=1}^3\mathrm{PaT}_i]/\sigma[\mathrm{PaT}] = 0.9280, \ \mathrm{rms} = 0.0037, \quad \text{(A35)} \\ &\sigma[\Sigma_{i=1}^3\mathrm{CaT}_i - 0.93\Sigma_{i=1}^3\mathrm{PaT}_i]/\sigma[\mathrm{CaT}^*] = 1.1397, \ \mathrm{rms} = 0.0078.\end{aligned}$$

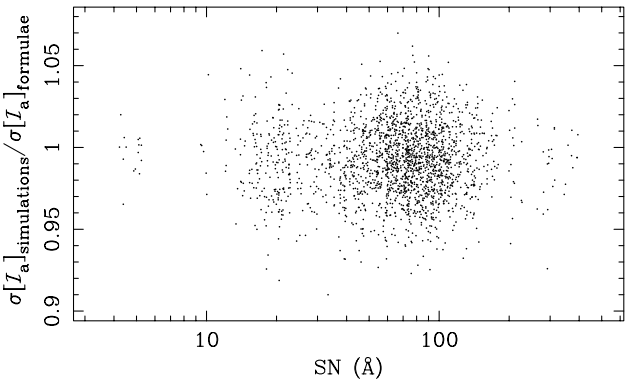

Figure A1. Comparison of absolute random errors in the measure of CaT, PaT and CaT* in the 706 stars of the library, obtained with the new formulae and with numerical simulations (1000 simulations per star and index were performed), as a function of the mean S/N ratio per angstrom in the bandpasses of each index. There is an excellent agreement, within statistical errors, between both methods (the mean $\sigma[\mathcal{I}_\mathrm{a}]_\mathrm{simulations}/\sigma[\mathcal{I}_\mathrm{a}]_\mathrm{formulae}$ value for the 2118 points is 0.99, with a rms of 0.02).

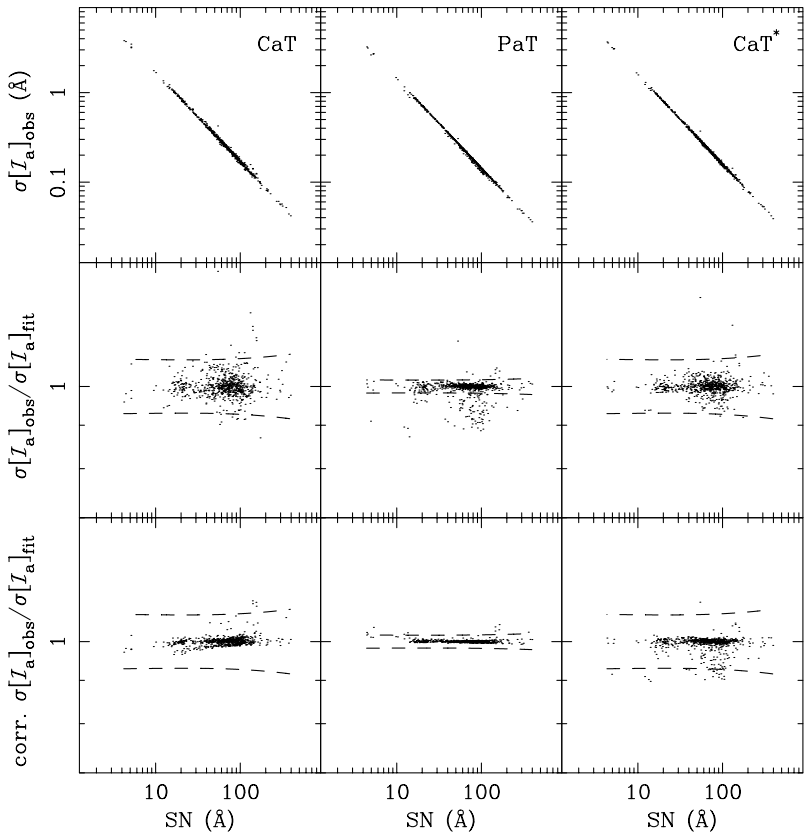

Figure A2. (*Top panels*) Absolute errors in the generic indices CaT, PaT and CaT*, measured in the 706 stars of the library, as a function of the S/N ratio per angstrom. (*Middle panels*) Residuals of a least-squares linear fit (rejecting data iteratively outside the 99.73 per cent confidence level – indicated by the dashed lines). (*Bottom panels*) Corrected residuals, obtained by correcting the initial residuals using the relations given in equation (A37).

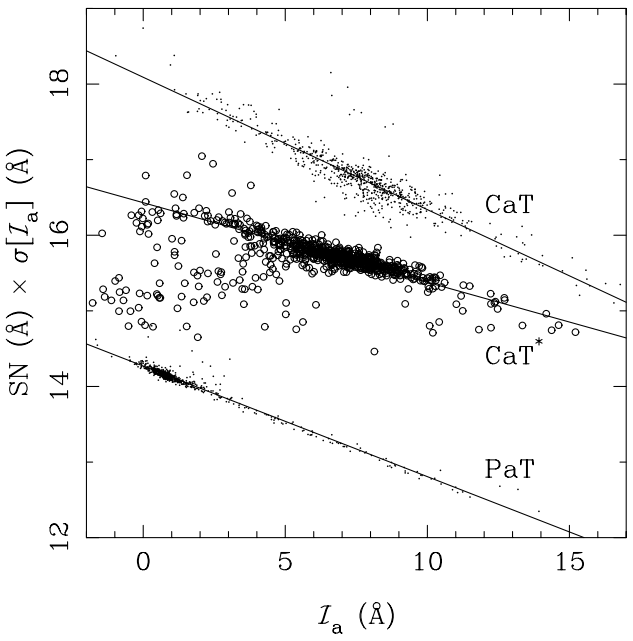

Figure A3. Empirical estimation of the constant factors c_1 and c_2 of equation (A36). The scatter for low CaT* data is due to stars with comparable CaT and PaT indices, which translates into relatively small CaT* values, but errors corresponding to indices with a larger absolute value. The least-squares fits to straight lines have been performed rejecting data iteratively outside the 99.73 per cent confidence level.

Summarizing, covariant terms, computed as given by equation (A26), must be retained in order to guarantee that random errors are free from systematic uncertainties.

A3 Estimation of random errors from S/N ratios

As we have already mentioned, it is possible to obtain estimates of the absolute errors of the classical indices as functions of the S/N ratio, using expressions as simple as equations (A7) and (A8). These formulae constitute a useful tool for observation planning. Unfortunately, the approximations employed to derive such expressions (see details in Cardiel 1999) cannot be used in the case of generic indices. For this reason we have decided to use an empirical approach to this problem.

In Fig. A2 (top panels) we represent the absolute errors in CaT, PaT and CaT* as a function of the average S/N ratio per angstrom, for the 706 stars of the library. An apparently tight correlation is shown by the three indices, as is expected. The residuals of a least-squares fit (middle panels) reveal that the dispersions of errors (rms) from the linear fit are 3.3, 2.6 and 2.3 per cent for the CaT, PaT and CaT* indices, respectively. Although this linear behaviour is a good first estimation of random errors for the generic indices, taking into account that the error estimation of classical atomic indices depends on the index value, we have investigated whether a relationship of the form

$$\sigma[\mathcal{I}_a] \simeq \frac{c_1 - c_2\mathcal{I}_a}{\mathrm{SN(\mathring{A})}} \qquad \text{(A36)}$$

can also be employed with the generic indices. For this purpose, we have represented in Fig. A3 the product $\mathrm{SN(\AA)} \times \sigma[\mathcal{I}_a]$ as a function of the index value, for the stellar library. It is clear that a good linear relation is exhibited by the three measured indices. The result of a least-squares fit to the data is

$$\sigma[\mathrm{CaT(\AA)}] \simeq \frac{18.09 - 0.1751\,\mathrm{CaT}}{\mathrm{SN(\AA)}},$$

$$\sigma[\mathrm{PaT(\AA)}] \simeq \frac{14.27 - 0.1463\,\mathrm{PaT}}{\mathrm{SN(\AA)}}, \tag{A37}$$

$$\sigma[\mathrm{CaT^*(\AA)}] \simeq \frac{16.43 - 0.1052\,\mathrm{CaT^*}}{\mathrm{SN(\AA)}}.$$

Since the fitted c_1 coefficients are two orders of magnitude larger than c_2, the dependence of generic index errors on the index values is not strong. However, the application of the relations given in equation (A37) reduces the residuals showed in Fig. A2 (bottom panels) for the CaT and PaT indices (rms 1.3 and 0.4 per cent, respectively), although it maintains those for the CaT* (rms 2.3 per cent).

The variation of the coefficients c_1 and c_2 with redshift, for classical indices, is described by (Cardiel 1999)

$$\begin{aligned} c_1|_z &= (1+z)^{1/2} c_1|_{z=0}, \\ c_2|_z &= (1+z)^{-1/2} c_2|_{z=0}, \end{aligned} \tag{A38}$$

where $c_1|_z$ and $c_2|_z$ are the coefficients to be employed in the spectra with redshift z, whereas $c_1|_{z=0}$ and $c_2|_{z=0}$ are the corresponding values at zero redshift. We have verified that this is also the case for the generic indices CaT, PaT and CaT* (for this purpose, we translated the 706 stellar spectra of the library as a function of fictitious redshifts, while maintaining the S/N ratio per angstrom). Therefore, the inclusion of the redshift effect in equation (A36) leads to

$$\begin{aligned} \sigma[\mathcal{I}_a]_z &\simeq \frac{c_1|_z - c_2|_z \mathcal{I}_a|_z}{\mathrm{SN(\AA)}} \\ &= (1+z)^{1/2} \frac{c_1|_{z=0} - c_2|_{z=0} \mathcal{I}_a|_{z=0}}{\mathrm{SN(\AA)}}, \end{aligned} \tag{A39}$$

where we have made use of the index variation with redshift given in equation (A32). Note that although the absolute error increases with redshift, the contrary is true for the relative error, i.e.

$$\left.\frac{\sigma[\mathcal{I}_a]}{\mathcal{I}_a}\right|_z = (1+z)^{-1/2} \left.\frac{\sigma[\mathcal{I}_a]}{\mathcal{I}_a}\right|_{z=0}. \tag{A40}$$

It is important to highlight that the relations given by equation (A37) should only be used to obtain approximate estimates of the generic index errors, and that they should not be considered as a substitution of the accurate formulae described in the previous section. In fact the application of approximated equations can lead to misleading index errors (see example in CGCG).

APPENDIX B: RESIDUAL RANDOM ERRORS

When the unbiased standard deviation of index measurements of stars with multiple observations, $\sigma[\mathcal{I}_a]_{\mathrm{rms}}$, is significantly larger than the expected typical error for the whole run $\sigma[\mathcal{I}_a]_{\mathrm{expected}}$, we derive a residual random error, $\sigma[\mathcal{I}_a]_{\mathrm{residual}}$ by the classical quadratic addition of errors

$$\sigma^2[\mathcal{I}_a]_{\mathrm{residual}} = \sigma^2[\mathcal{I}_a]_{\mathrm{rms}} - \sigma^2[\mathcal{I}_a]_{\mathrm{expected}}. \tag{B1}$$

Although a straight procedure would be to add quadratically the residual term to the random error of each star, we preferred to introduce it through a multiplicative factor in order to keep the original relative qualities among the stars, getting at the same time reliable error spectra that can be used for any index definition. The introduction of such a factor is justified since, as we have shown in Appendix A3, random errors of the generic indices CaT, PaT and CaT* can be derived from analytical functions of the index value and the S/N ratio [see equation (A37)]. Thus, we consider that the effect of increasing the random errors is equivalent to enlarging the photon noise N_k of each star to a new value N_k^* by multiplying with a factor $f > 1$

$$N_k^* = f N_k, \quad \text{and therefore} \tag{B2}$$

$$\mathrm{SN}_k^*(\mathrm{\AA}) = f^{-1}\mathrm{SN}_k(\mathrm{\AA}) \tag{B3}$$

where k refers to the kth star. By substituting equation (B3) in equation (A36), it is immediate to show that the final random error, $\sigma[\mathcal{I}_a]_{\mathrm{final},k}$, can be computed as

$$\sigma[\mathcal{I}_a]_{\mathrm{final},k} \simeq f\sigma[\mathcal{I}_a]_{\mathrm{expected},k}. \tag{B4}$$

Next, and in order to derive an analytical expression of f, the quadratic addition of errors and equation (B4) are simultaneously considered:

$$\begin{aligned} \sigma^2[\mathcal{I}_a]_{\mathrm{final},k} &= \sigma^2[\mathcal{I}_a]_{\mathrm{residual}} + \sigma^2[\mathcal{I}_a]_{\mathrm{expected},k} \\ &\simeq f^2\sigma^2[\mathcal{I}_a]_{\mathrm{expected},k}, \end{aligned} \tag{B5}$$

which leads to a initial expression of f

$$f \simeq \sqrt{1 + \frac{\sigma^2[\mathcal{I}_a]_{\mathrm{residual}}}{\sigma^2[\mathcal{I}_a]_{\mathrm{expected},k}}}. \tag{B6}$$

Note that equation (B6) is not definitive since it depends on the expected random error of each star. An approximated general expression is finally obtained by substituting the individual errors by the expected typical error for the whole run

$$f \simeq \sqrt{1 + \frac{\sigma^2[\mathcal{I}_a]_{\mathrm{residual}}}{\sigma^2[\mathcal{I}_a]_{\mathrm{expected}}}}. \tag{B7}$$

This paper has been typeset from a TEX/LATEX file prepared by the author.